HELVETICA chimica acta

Design of A Metabolically Stable Tritium-Tracer of the PI3Kδ-Inhibitor CDZ173 (Leniolisib) as a Tool to Study Liver Metabolites

Carsten Bauer,*[a,1] Tong Luu,[a] Fabian Eggimann,[b] Patrick Bross,[a] Werner Gertsch,[c] Cheng Hu,[b] Philippe Ramstein,[c] Julien Bourgailh,[c] Albrecht Glänzel,[a] Ina Dix,[b] Christian Guenat,[b] Nicolas Soldermann,[b] Karine Litherland,[c] Sandrine Desrayaud,[c] Jean-Claude Hengy,[c] David Pearson,*[c] Joachim Blanz,[c] and Christoph Burkhart[d]

[a]Isotope Laboratory, PK Sciences, Novartis Institute for Biomedical Research (NIBR), Basel, e-mail: carsten.bauer@unibas.ch
[b]Global Discovery Chemistry, NIBR, Basel
[c]ADME Biotransformation, PK Sciences, NIBR, Basel, e-mail: david.pearson@novartis.com
[d]Autoimmunity, Transplantation and Inflammation, NIBR, Basel

In this disclosure, we summarize the preliminary metabolic profiling of the PI3Kδ inhibitor CDZ173 (leniolisib, **1a**) obtained from incubations of the unlabeled compound and the synthesis of its metabolically stable tritium isotopologue **1b** used for metabolite structure confirmation. Access to **1b** was achieved when a halogenated precursor was subject to Hal/^{3}H-exchange. Hence, [^{3}H]CDZ173 with specific activity 630 GBq/mmol, HPLC-RA 97% and *ee* = 99.2% was obtained. Synthetic key to the precursor was using a bis-halo-pyridine in a Pd-catalyzed mono-amination of the tetrahydropyrido-pyrimidine core. Stereochemistry of the synthetic precursors were confirmed by X-ray analysis of the unlabeled bis-halo-pyridines and chiral HPLC of the tritiated material. The correct position of tritium label in the target, was confirmed by ^{3}H-NMR difference spectroscopy. Besides, we report on the validation of the radiotracer as a tool for pre-clinical ADME in incubations with hepatocytes. Based on this data, we present a quantitative metabolite profile of leniolisib which was confirmed by independently synthesized metabolite references. The conformation of CDZ173 was investigated by NMR suggesting two different amide backbones each with specific pyrrolidine puckerings.

Keywords: PI3Kδ inhibitor, leniolisib, CDZ173, metabolism of pyrrolidines, conformational analysis of pyrrolidines.

Introduction

Since its discovery in 1985,[1] phosphatidylinositide 3-kinases (PI3K) have become important drug targets in medicinal chemistry. Recently we have discovered the 7-phenyl-2-pyyrolidinyloxy-quinoxaline CDZ173 (leniolisib; **1a**), which is a promising PI3Kδ inhibitor and conformationally flexible side chain with (*S*)-stereochemistry.[2] Most recently, leniolisib was investigated in a 12-week, open-label and within-subject dose-escalation study in patients with Activated PI3K Delta Syndrome (APDS).[3] Leniolisib led to a dose-dependent reduction in PI3K/Akt pathway activity assessed *ex vivo* and improved immune dysregulation and it may be a new treatment option for patients with pathological activation of the PI3Kδ pathway, as in B cell malignancies or autoimmune disorders including *Sjögren*'s syndrome, systemic lupus erythematosus or rheumatoid arthritis.

To summarize,[4 – 6] starting from the lead compound BEZ522 sophisticated SAR studies yielded the 3rd generation PI3Kδ inhibitor CDZ173 with improved biophysical properties, promising PK/PD and encouraging clinical results. As part of the preclinical program, the ADME properties of this compound were investigated in animal models. For these studies it was aimed[7] to use a more economical and metabolically stable tritium analogue of CDZ173 as a very sensitive, weak β^- emitting radiotracer for the

[1] Current address: Department of Chemistry, University of Basel, Biopark BPR 1096, Mattenstrasse 24a, CH-4058 Basel, e-mail: carsten.bauer@unibas.ch

quantification of metabolites and elimination routes with a low cost radiolabel. The development of this radiotracer for preclinical studies is described in the following sections.

Results and Discussion

Defining the Ideal Position for ^{3}H-Labelling of CDZ173 Based on Metabolites Found After Microsomal Incubation

Prior starting the synthesis work on [^{3}H]CDZ173 (**1b**), metabolic profiling data of unlabeled CDZ173 was acquired in order to define the most likely metabolically stable proton/tritium position in CDZ173 (see *Supplementary data* for Materials And Methods). Since members of the CYP-enzyme family account for 75% of drug metabolism,[8] liver microsomes are a practical system to determine metabolic stability of most compounds. Information on the elimination pathways of a drug can be obtained by analyzing bile and urine in animal models. Hence, for metabolic profiling, unlabeled CDZ173 was incubated with liver microsomes of rat, mouse, dog, cynomolgus monkey and human and administered to bile-duct cannulated rat with collection of blood, bile, urine as well as tissues at necropsy. Subsequently, the samples of the *in vitro* incubations as well as of the animal model were analyzed by LC/MS/MS.

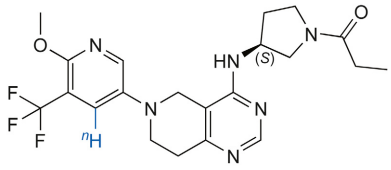

1a n = 1 (CDZ173, Leniolisib)
1b n = 3 [^{3}H]CDZ173

A total of about 50 microsomal metabolites were detected, but metabolic profiling and preliminary structure investigations were limited to 26 microsomal metabolites $M_M1 - M_M26$ with larger LC/MS peak areas (*Table 1*). LC/MS-Peak areas of the microsome incubations and body/tissue-samples of the metabolites were determined but will not be discussed here, because no reference standards were used in this preliminary analysis. Isomeric xenobiotics were distinguished by the characteristic LC-retention time (*e.g.* M_M3 and M_M15). The numbering of the metabolites is given by their sequence of retention times (LC t_R). *Table S1* (for space reasons placed in the *Supplementary Material*) summarizes the data gathered from MS/MS^n spectrometry of the metabolites. In this table, *column 4* lists the proposed structure and molecular formula, and *column 5* lists the observed $[M + H]^+$. *Columns 7 – 11* list *m/z* in MS^2 and MS^3 together with the assigned cations.

O-Demethylation, amide bond hydrolysis (*group A*), C-oxidation at the tetrahydropyrido moiety, at the pyrrolidine moiety, as well as mixed oxidation at both moieties were identified as important biotransformation steps (*groups B, C, E – H*). Oxidation at the pyrrolidine moiety also led to ring opening and subsequent oxidation of the aliphatic side chain to the corresponding acid (*group D*). N-Oxidation was not detected among the metabolites that were subject of structure elucidation.

To summarize, the 26 detected metabolites can be grouped in seven structural categories *A – H*. The molecular mass of several metabolites indicated a loss of two, in one case four hydrogens that may be attributed to an initial oxidation and a subsequent loss of a water molecule during the ionization process. For this reason, such metabolites (*e.g.* M_M8 or M_M12) are grouped together with hydroxylation metabolites. Based on its fragmentation pattern and the characteristic loss of *m/z* 176,[9] M_M14 was assigned to be a glucuronide. Reactive intermediate trapping with glutathione was performed but glutathione adducts were not detected in any of the microsomal incubations. However, a cysteine conjugate[9] (M_M17) was detected in all *in vivo* samples. Hence in *Table 1* these two conjugates are treated as a follow up products of a hydroxylated species; for more explicit structures, see the structure of the corresponding metabolite in *Table 12.1* in the *Supplementary Material*.

Most importantly, no metabolites with hydroxylation at the pyridine ring-carbon were observed. It was shown that CDZ173 is extensively metabolized at the tetrahydropyridopyrimidine (THP), the pyrrolidine and O-methyl group, but not at the CF_3-containing pyridine ring. A very similar metabolic inertness was found for the *m*-CF_3-pyridine moiety in the *in vitro* and *in vivo* metabolism of the cannabinoid-1 receptor inverse antagonist taranabant.[10] Thus, the most important scope of this analysis was achieved. This was to define the synthetic target for later tritium positioning. Based on this reasoning and the first metabolic profiling data summarized here, the synthetic target structure for radiolabeling was defined to be **1b** (*Figure 1*).

Synthesis of the [^{3}H]Tracer

Development of the Precursor Synthesis Suitable for End-Tritiation. The medicinal chemistry of CDZ173 was published in 2017.[2] There, the synthesic route for CDZ173 consists out of three principal steps, which are

Table 1. Structure categories of microsomal metabolites of CDZ173

Category of M	Biotransformation step	Narrowed structures	Metabolites
A	Demethylation and hydrolysis	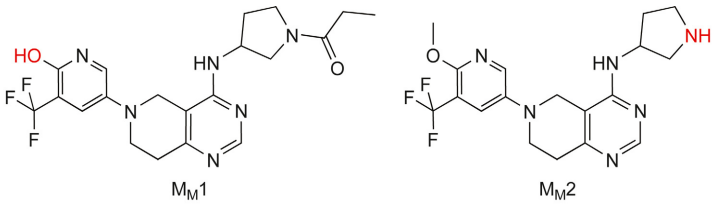	M_M1, M_M2
B	Pyrrolidine mono-hydroxylation	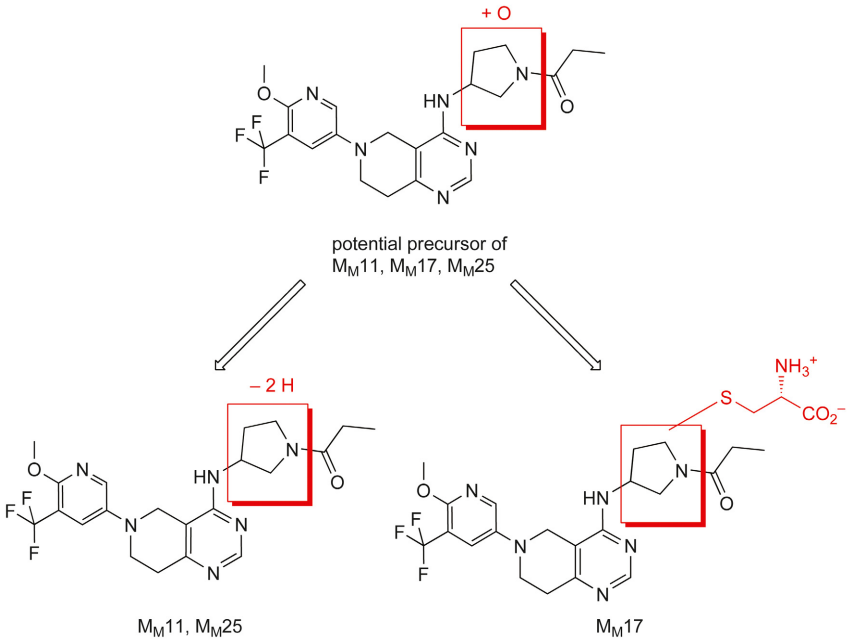	M_M11, M_M17, M_M25
C	N-propionly-pyrrolidine mono-hydroxylation	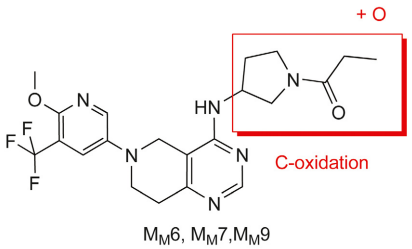	M_M6, M_M7, M_M9
D	Formal hydration and oxidation	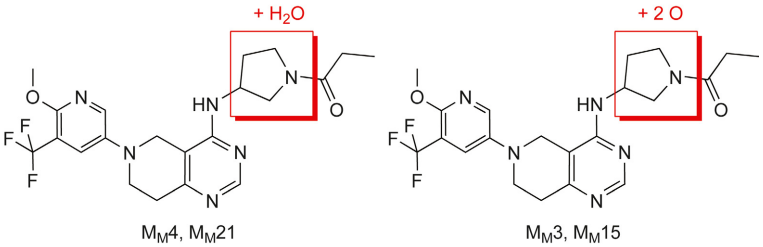	M_M3, M_M4, M_M15, M_M21

Table 1. (cont.)

Category of M	Biotransformation step	Narrowed structures	Metabolites
E	Pyrrolidine bis-hydroxylation	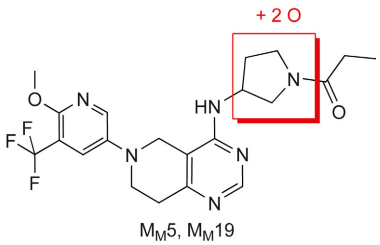 M_M5, M_M19	M_M5, M_M19
F	THP mono-hydroxylation	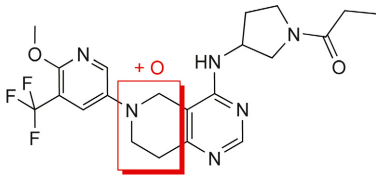 M_M10, M_M22	M_M10, M_M22
G	THP bis-hydroxylation	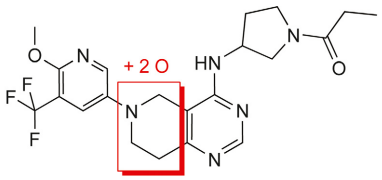 M_M8, M_M12, M_M13, M_M14, M_M23, M_M26	M_M8, M_M12, M_M13, M_M14, M_M23, M_M26
H	Pyrrolidine and THP bis-hydroxylation	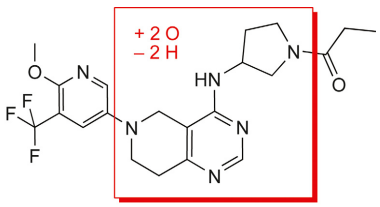 M_M16, M_M18, M_M19, M_M20, M_M24	M_M16, M_M18, M_M19, M_M20, M_M24

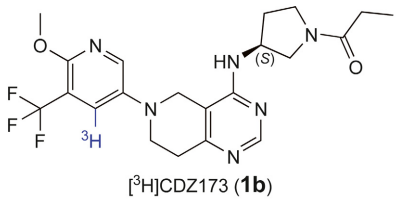
[^{3}H]CDZ173 (**1b**)

Figure 1. Structure of the radiosynthesis target [^{3}H]CDZ173.

a) the amination of an extended 4-chloropyrimidine with a by-functional aliphatic amine, *b*) the extension of the pyrimidine system by Pd-catalyzed amination using a X-Phos ligand and a poly-substituted pyridine, and *c*) completion of the targets by further modification on the by-functional amine mentioned under *a*). For a comprehensive synthesis scheme of the medicinal chemistry synthesis of CDZ173, see the Supplementary part of reference [2].

For radiosynthesis, *i.e.*, introduction of the tritium in the very last step of the synthesis, this general approach needed to be changed as outlined in *Scheme 1*. The radiosynthesis started from the *N*-protected 5,6,7,8-tetrahydropyrido[4,3-*d*]pyrimidin-4-ol **2**,[11] which was transformed into the corresponding chloride **3**. Subsequent nucleophilic substitution with the amine **6** in step *ii* gave **7**. Debenzylation in step *iii* gave **8**. In order to confirm the chiral purity of **8**, an analytical sample was BOC-protected and analyzed by chiral HPLC. It became clear that slight racemization had occurred in step *iii*. For this reason, racemized **8** was BOC-protected to yield **9**. Slightly racemized **9** was purified by preparative chiral HPLC (step *v*) to

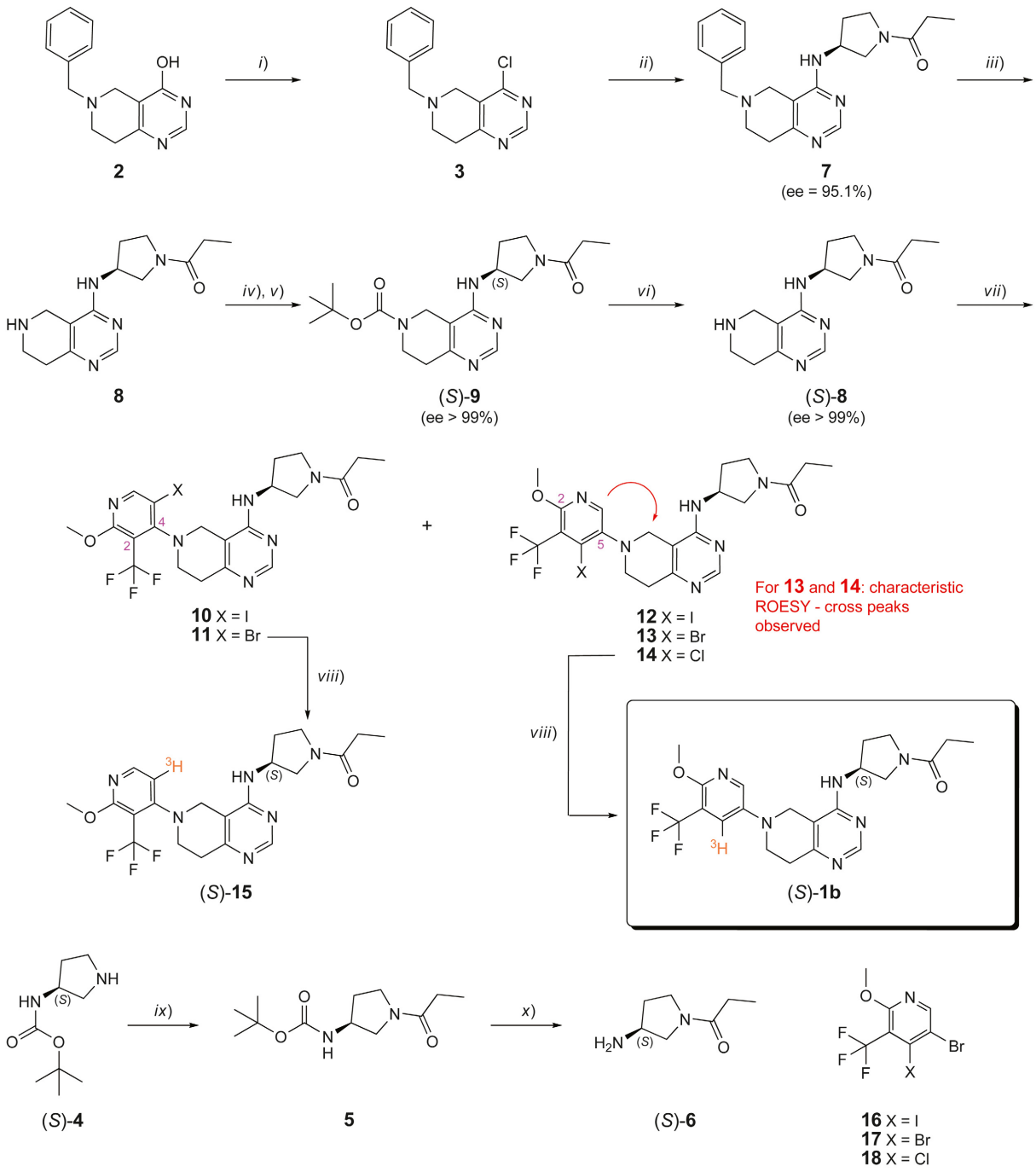

Scheme 1. Synthesis of [^{3}H]CDZ173. Reagents and conditions: *i*) $POCl_3$, Et_3N, Tol, 100 °C, 2 h; *ii*) (*S*)-**6**, EtOH, AcOH, 140 °C, 16 h; *iii*) $Pd(OH_2)$ on C, H_2 (gas), EtOH, 60 °C, 16 h; *iv*) Boc_2O, Et_3N, CH_2Cl_2, 0 °C → r.t., 3 h; *v*) preparative chiral purification; *vi*) 1. HCl, Et_2O, 0 °C → r.t., 2 h; 2. 1 M NaOH, THF/MeOH; *vii*) see *Table 2* for conditions used for X = I, Br, and Cl; *viii*) 10% Pd on C, DIPEA, 19 mbar T_2-gas, DMF, 150 °C, 2 h; *ix*) $Cl(CO)CH_2CH_3$, Et_3N, THF, r.t., 2 h; *x*) 4 M HCl, CH_2Cl_2, r.t., 2 h.

yield – after the removal of the BOC group (step *vi*) – optically pure (*S*)-**8**. This precursor was used for palladium-catalyzed amination with the bis-halides **16**, **17**, and **18**. The pyridines **16**, **17**, and **18** were prepared by metalation of the CF_3-pyridine core using LDA as super base[12][13] and iodine, $C_2Br_2Cl_4$, or C_2Cl_6 as source for electrophilic halogen (El). *Table 2* summarizes the conditions under which these pyridines were obtained. In order to avoid by-products due to transmetalation and/or iodine-migration[14] strict temperature control was applied with the result that stereochemically pure **16** was obtained (*Entry 1*; see

Table 2. Experimental conditions for site-selective metalation of the halo-pyridines **16**, **17**, and **18** and subsequent electrophile trapping

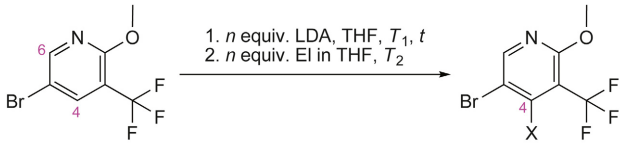

16 X = I
17 X = Br
18 X = Cl

X	n	T_1 [°C]	t [min]	El	equiv. of El	T_2 [°C]	Yield[a]	Remark
I (**16**)	1.0	< −90	180	I_2	1.5 (in portions)	−75	60%	Cat. amount of LiBr was present and control of T_1 and T_2
I (**16**)	2.5	−75	45	I_2	4.0	0	45%	
Br (**17**)	2.0	−75	45	$C_2Br_2Cl_4$	2.0	0	20%	
Cl (**18**)	2.5	−75	45	C_2Cl_6	2.0	0	48%	

[a] Yield and stereochemical purity were determined by GC-MS.

Supplementary Material for GC-MS of **16** prior to chromatography). However, under these conditions only 60% starting material conversion was observed. Hence, since chromatography needed to be applied anyway to isolate the product, an excess of LDA was used in subsequent preparations (*Entries 2 – 4*). X-Ray data of **16**, **17**, and **18** are shown in the *Supplementary Material* to ultimately prove the stereochemical identity of these building blocks.

In subsequent chemical methodology experiments, (*S*)-**8** was coupled under *Buchwald–Hartwig* conditions with either of the bis-halogenated pyridines in step *vii*. Goal of this methodology sub-project was to test to which extend a C(5)-coupling product can be favored if two halogens on C(4) and C(5) are present. Since the reaction rate of the following step *viii*, hence the later content of tritium and the specific activity in **1b** depends on the decreasing bond strength between a sp^2-carbon and a halogen X (C–Cl > C–Br > C–I),[15] achieving C(5)-coupling selectivity during the amination step with the iodide and the bromide was prioritized first.

Table 3 summarizes the conditions applied in the amination step (*vii*) using the substrates **16** – **18**.[16 – 18] When the pyridine-iodide **16** and the pyridine-bromide **17** were used as coupling substrates (*Entries 1* and *2*), the C(5)-coupling products **12** (iodide) and **13** (bromide) were found in traces in the crude mixtures (see *Supplementary Material* for analytical data). ROESY- and HMBC-experiments of a 95:5-mixture of the bromides **11** and **13** indicated the presence of **13** by cross peaks characteristic for this isomer (see *Scheme 1* and

Table 3. Palladium catalyzed amination conditions tested to achieve C(5)-selectivity

Entry	Pyridine	Amine	Catalyst system	Ratio C(4)–N:C(5)–N[a]
1	**16** (X = I)	(*S*)-**10**	$Pd_2(dba)_3$, BINAP, KF on Al_2O_3, solvent free, 120 °C, MW @ 240 W, 2 h,[17] low yield	> 99:1
2	**17** (X = Br)	(*S*)-**10**	$Pd_2(dba)_3$, BINAP, Cs_2CO_3, dioxane, 135 °C, MW @ 240 W, 2 h,[16] < 5% yield isolated as fraction with C(5)-isomer enrichment	*ca.* 95:5
3	**17** (X = Br)	(*S*)-**10**	$Pd_2(dba)_3$, ^{t}BuMePhos, NaO^{t}Bu, ^{t}BuOH, 100 °C, 4 h[18] (higher yield in crude product mixture)	*ca.* 95:5
4	**17** (X = Br)	TIQ[b]	$Pd_2(dba)_3$, $Me_4{}^t$BuPhos, NaO^{t}Bu, ^{t}BuOH, 100 °C, MW @ 230 W, 3 h	No reaction
5	**18** (X = Cl)	(*S*)-**10**	$Pd_2(dba)_3$, ^{t}BuMePhos, NaO^{t}Bu, ^{t}BuOH, 100 °C, 4 h, 6% isolated	> 1:99

[a] *Entry 1* and *3*: ratio of isomers determined by LC/MS in the crude mixture. In case of *Entry 1*, the structure of the isomer is given by the substitution pattern of the pyridine **23**. *Entry 2*: ratio of isomers was determined by LC/MS of the enriched fraction. *Entry 5*: isomer ratio in the crude product is estimated since compound **29** was the only isomer which could be isolated. [b] Tetrahydroisoquinoline (TIQ) was used as a synthetic model for the amine **10**.

Supplementary Material). However, when the 95:5 mixtures of **11** and **13** was tritiated, the small about of tritiated **1b** (from **13**) was lost during preparative HPLC purification (no RA detector could be used). Consequently, the major product (*S*)-**15** was isolated and characterized by correct mass peak but a different HPLC-retention time as required for [^{3}H]CDZ173.

In an attempt to favor C(5)-N amination over C(4)-N amination occurring next to the bulky, vicinal CF_3-group on Py, the sterically more demanding ligand $Me_4{}^tBuPhos$ with tetramethylation on phosphine bearing phenyl was tested. This hypothesis however was falsified (*Table 3*, *Entry 4*). Since none of the known ligands and catalyst systems tested in step *vii* provided the stereoelectronic effects on the transition metal needed to achieve C(5)-coupling product enrichment and since HPLC-isolation of **1b** from a mixture of (*S*)-**15** and **1b** was impossible, tritiating either **12** or **13** needed to be abandoned. Instead, when the relatively easy accessible chloro-pyridine **18** was used in step *vii*, the CDZ173-derivative **14** was the only coupling product to be observed in step *vii*. The isolated amount of **14** (< 10% yield) was sufficient to complete the tritiation within this project.

Radiosynthesis. In order to cope with the analytical requirements of metabolic profiling from a regulatory perspective,[19] radioanalytical tools are needed, that provide excellent sensitivity. Typically, the limit of detection of a tritium-labelled analyte it is 0.2 – 0.7 Bq (10 – 40 dpm).[20] Practically this means, that a tritium-tracer is able to detect the xenobiotic analyte in a pico- to femtomolar range allowing accurate and sensitive determination of metabolism pathways in ADME studies.

Upon Cl-tritium exchange on **15** in step *viii*, the radiotracer **1b** was obtained after purification with a specific activity of 0.623 TBq/mmol after purification. The correct position of the ^{3}H-label was confirmed by 1D-^{3}H-NMR (spectra not shown; *singulet* at δ (^{3}H) = 7.87 ppm) and compared with the value of the fully assigned, unlabeled material (δ(^{1}H) = 7.87 ppm; see *Experimental Section*). The radiochemical yield of 58% referred to 1 × 100% tritium-labeling in one position (max. 1.08 TBq/mmol possible) seems to be small compared to a hypothetical iodine-tritium exchange with *ca*. 90% radiochemical yield. However, considering the requirements of analytical chemists on the minimum specific activity of radiotracers in general,[21] the presumably metabolically stable tracer **1b** with a specific activity = 0.623 TBq/mmol (undiluted) has a limit of detection in the attogram range of the analyte. Hence, in this context, the interesting question of C(4)/C(5)-coupling selectivity for getting access to the halogenides **12** and **13** in practical yields became less important during the ongoing of the project. Nevertheless, a synthetic tool was provided which can fulfil the requirements of bioanalysts as discussed above.

Validation of the ^{3}H-Tracer as ADME-Tool by Incubation with Hepatocytes

In order to test the metabolic stability of [^{3}H]CDZ173 and validating it as a potential tool for ADME-studies, a sample of **1b** with a specific activity of 630 MBq/mmol was diluted 1:50 with the phosphate salt of unlabeled CDZ173 ($[C_{21}H_{26}F_3N_6O_2]^+[H_2PO_4]^-$). Micrograms of this diluted material were incubated with cryopreserved hepatocytes from rats and humans at 5 μM concentrations for up to 4 h and the incubate profiles were analyzed by UPLC with radioactivity detection. *Figure 2* shows the incubation profile after 4 h in rat hepatocytes (ratHEP) and human hepatocytes (huHEP). The metabolism of this diluted material in rat and human hepatocyte incubations showed the formation of eleven phase I metabolites. The following baseline separated hepatic metabolites M_H were analyzed by LC/MS and LC/MS^2 on a *Q-ToF Synapt I* mass spectrometer: M_H14, M_H16, M_H1, M_H14, M_H4, M_H3, M_H10, M_H21, M_H5, M_H6, M_H7, M_H25, and M_H9. In this row, the metabolites are ordered according to their retention time (see *Table 4*, column 2 for values of t_R and column 11 for relative peak areas). It was observed that CDZ173 is heavily metabolized in human and rat hepatocytes with M_H1 and M_H5 being the most abundant. Metabolite structural information was obtained to evaluate the metabolically stability of the isotopomer of [^{3}H]CDZ173 shown in figure 6. In column 4 of *Table 4*, the elementary composition of the M_H calculated from the observed $[M + H]^+$ (column 6) is listed. It is compared with the calculated exact mass for $[M + H]^+$ (column 5) to give the deviation of the observed *m/z* (in ppm) relative to the calculated value (column 7). For possible interpretations and individual MS^1/MS^2 +ESI high resolution spectra of the metabolites obtained from hepatocyte incubations: see *Supplementary Material*.

Structural Conclusions from ESI+ Fragmentation Patterns of Hepatocyte Metabolites M_H and Metabolite Clustering

Reference CDZ173. Our interpretation of the ESI-fragmentation of CDZ173 in the MS/MS^2 spectra captures earlier interpretations of MS-data of 1,2,3,4-tetrahydroisoquinolines (THQ).[22][23] In these studies, the fragmentation of the piperidine moiety in THQ

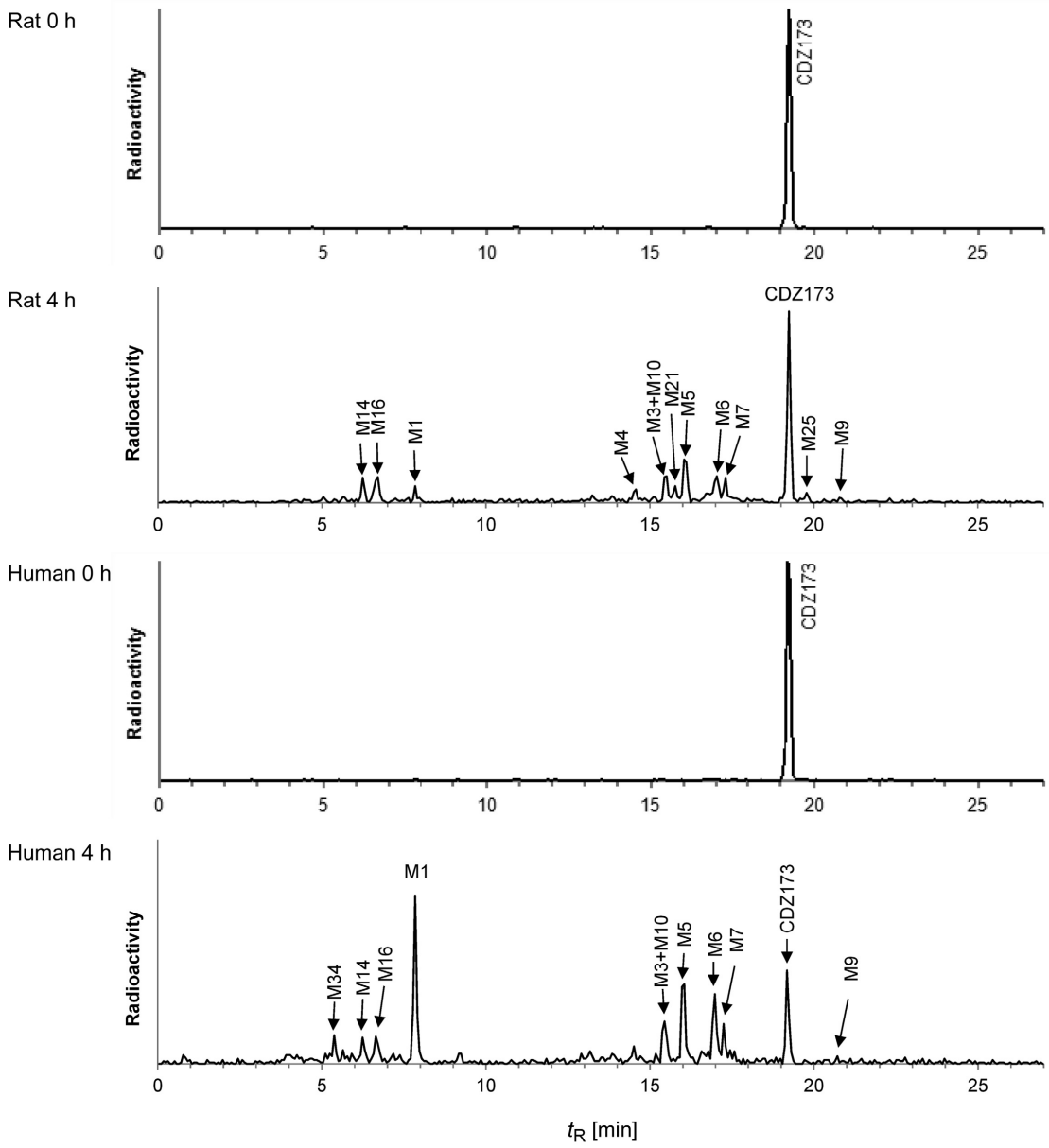

Figure 2. Profiles of the hepatic metabolites M_H of [^{3}H]CDZ173 after 4 h incubation with rat and human hepatocytes.[2]

was interpreted to occur *via* a retro *Diels–Alder* reaction (*rDA*). Yet, key to our interpretation of the ESI-MS data is the assumption that the tertiary, aromatic amine function in CDZ173 (Py-N-piperidine) should have a similar low $E_{1/2}$ as the model compound tetramethyl-*p*-phenyldiamine (TMPD; $E_{1/2} = -0.28$ V)[24] and therefore easily oxidizes to form a nitrogen centered radical initiating a rDA-process. To compare, the redox-potential of 4-amino-pyrimidine and pyridine was determined to be $E_{1/2} = -1.115$ and $E_{1/2} = 1.82$ V, respectively.[25] The peak potential (E_p) of *N,N′*-dimethylpropionamide was found to be $E_p = 1.26$ V.[26] Hence, oxidizing N(1) of pyrimidine in CDZ173 is unlikely.

The MS^2 of the unlabeled reference CDZ173 (*Figure 3*) shows $[M + H]^+$ at *m/z* 451.20 and structurally characteristic fragment ions at *m/z* 247.15, 191.13, and 174.1029. Below this, the fragment ions become noisy (*m/z* 147.09, 124.09, and 122.07), what we interpret as increasing tendency to form radicals and radical reaction products (*e.g. m/z* 149.09). One possible molecular interpretation of this fragmentation pattern is shown in *Scheme 2*. Upon oxidation of the piperidine nitrogen, a rDA in the THQ-moiety is postulated, which can explain *m/z* 247.15. This fragment ion depropionlyates to yield *m/z* 191.12. Subsequent elimination of

[2] For reasons of graphic clarity, the subscript 'H' is ignored in the annotations of *Figure 2*.

Table 4. Elementary composition of CDZ173 metabolites determined by high resolution LC/MS after incubation of diluted, 1% T-labelled [^{3}H]CDZ173 in rat and human hepatocytes (specific activity = 0.01265 TBq/mmol)

Metabolite M_{HEP}	t_R	Group	Calc. elemental composition of $[M + H]^+$	m/z_{calc} of $[M + H]^+$	m/z_{obs} in MS^1	Dev. m/z [ppm]	Assigned molecule ion in MS^1	m/z in MS^2	Assigned molecule ion in MS^2	Rel. peak areas [%] of the metabolite	
										ratHEP[b]	huHEP[b]
CDZ173	19.2	na	$[(C_{21}H_{25}F_3N_6O_2)H]^+$	451.2064	451.2067	+0.665	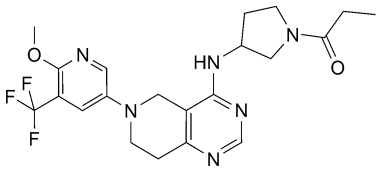	247.1897 191.1290 174.1026 124.0871 122.0713	$[C_{13}H_{19}N_4O]^+$ $[C_{10}H_{15}N_4]^+$ $[C_{10}H_{12}N_3]^+$ $[C_6H_{10}N_3]^+$ $[C_6H_8N_3]^+$	38.40	12.00
M_H1[a]	7.83	A′	$[(C_{20}H_{23}F_3N_6O_2)H]^+$	437.1907	437.1897	−2.287	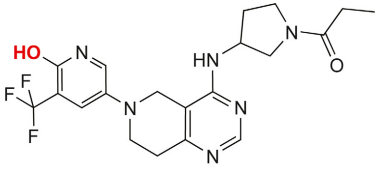	247.1897 191.1281 (−$C_3H_5O^+$) 124.0861	$[C_{13}H_{19}N_3O]^+$ $[C_{10}H_{15}N_4]^+$ $[C_6H_{10}N_3]^+$	2.59	21.50
M_H3[b]	15.4	E′	$[(C_{21}H_{25}F_3N_6O_4)H]^+$	483.1962	483.1965	+0.621	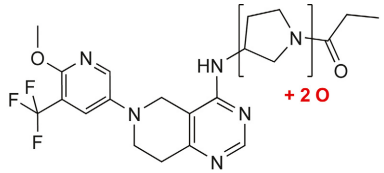	364.1476 279.1433 244.1324 206.0928 160.0845	$[C_{17}H_{17}F_3N_5O]^+$ $[C_{13}H_{19}N_4O_3]^+$ $[C_{13}H_{16}N_4O]^+$ $[C_{10}H_{12}N_3O_2]^+$ $[C_9H_{10}N_3]^+$	3.14	3.81
M_H4	14.5	D′	$[(C_{21}H_{27}F_3N_6O_3)H]^+$	469.2169	469.2169	±0	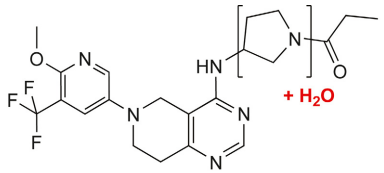	326.1194 265.1633 192.1145 174.1076 122.0742	$[C_{14}H_{15}F_3N_5O]^+$ $[C_{13}H_{21}N_4O_2]^+$ $[C_{10}H_{14}N_3O]^+$ $[C_{10}H_{12}N_3]^+$ $[C_6H_8N_3]^+$	2.68	1.83
M_H5	16.0	E′	$[(C_{21}H_{25}F_3N_6O_4)K]^+$ $[(C_{21}H_{25}F_3N_6O_4)Na]^+$ $[(C_{21}H_{25}F_3N_6O_4)H]^+$	521.1572 505.1782 483.1962	521.1503 505.1794 483.1974	−1.3239 +2.375 +2.482	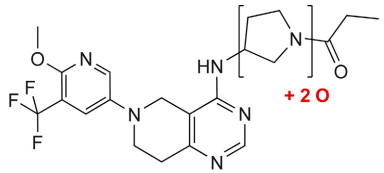	465.1815 279.1452 223.1158 194.0930 158.0728 122.0724	$[C_{21}H_{22}F_3N_6O_3]^+$ $[C_{10}H_{15}N_4O_2]^+$ $[C_9H_{12}N_3O_2]^+$ $[C_9H_8N_3]^+$ $[C_6H_8N_3]^+$	11.0	13.1

Table 4. (cont.)

Metabolite M_{HEP}	t_R	Group	Calc. elemental composition of $[M + H]^+$	m/z_{calc} of $[M + H]^+$	m/z_{obs} in MS^1	Dev. m/z [ppm]	Assigned molecule ion in MS^1	m/z in MS^2	Assigned molecule ion in MS^2	Rel. peak areas [%] of the metabolite	
										ratHEP[b]	huHEP[b]
M_H6	17.0	B′	$[(C_{21}H_{25}F_3N_6O_3)H]^+$	467.2013	467.2013	±0	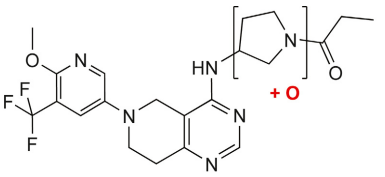	449.1912 393.1653 245.1412 189.1129 172.0872 160.0881	$[C_{21}H_{22}F_3N_6O_2]^+$ $[C_{18}H_{20}F_3N_6O]^+$ $[C_{13}H_{17}N_4O]^+$ $[C_{10}H_{13}N_4]^+$ $[C_{10}H_{10}N_3]^+$ $[C_9H_{10}N_3]^+$	7.35	13.10
M_H7	17.3	B′	$[(C_{21}H_{25}F_3N_6O_3)\ Na]^+$ $[(C_{21}H_{25}F_3N_6O_3)H]^+$	489.1838 467.2013	489.1832 467.2030	−1.226 +3.639	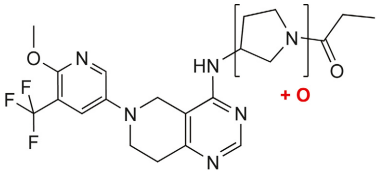	449.1912 393.1645 245.1391 189.1129 172.0872 160.0881	$[C_{21}H_{22}F_3N_6O_2]^+$ $[C_{18}H_{20}F_3N_6O]^+$ $[C_{13}H_{17}N_4O]^+$ $[C_{10}H_{13}N_4]^+$ $[C_{10}H_{10}N_3]^+$ $[C_9H_{10}N_3]^+$	4.39	4.55
M_H9[a]	20.7	X′	$[(C_{21}H_{25}F_3N_6O_3)H]^+$	467.2018	467.2018	±0	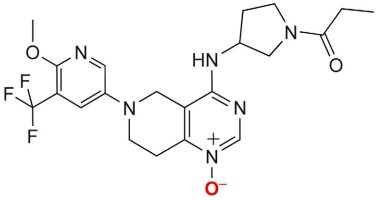	435.1817 324.1045 298.0698 263.1514	$[C_{21}H_{24}F_3N_5O_2]^+$ $[C_{14}H_{13}F_3N_5O]^+$ $[C_{13}H_{19}N_4O_2]^+$ $[C_{13}H_{13}F_3N_4O]^+$	0.65	0.27
M_H10[b]	15.5	C′	$[(C_{21}H_{25}F_3N_6O_3)H]^+$	467.2013	467.2021	+1.712	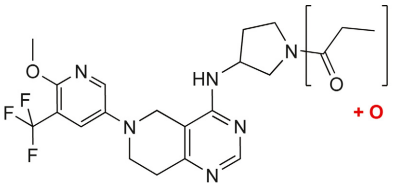	263.1488 191.1253 176.0704	$[C_{13}H_{19}N_4O_2]^+$ $[C_9H_{12}N_4]^+$ $[C_9H_{10}N_3]^+$	4.39	4.55
M_H14	6.27	B′	$[(C_{20}H_{23}F_3N_6O_3)Na]^+$ $[(C_{20}H_{23}F_3N_6O_3)H]^+$	475.1681 453.1856	475.1648 453.1894	+6.945 +8.385	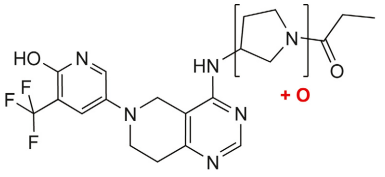	435.1762 379.1458 189.1167 172.0883	$[C_{20}H_{24}F_3N_6O_2]^+$ $[C_{10}H_{13}N_4]^+$ $[C_{10}H_{10}N_3]^+$	4.30	3.15

Table 4. (cont.)

Metabolite M_{HEP}	t_R	Group	Calc. elemental composition of $[M + H]^+$	m/z_{calc} of $[M + H]^+$	m/z_{obs} in MS^1	Dev. m/z [ppm]	Assigned molecule ion in MS^1	m/z in MS^2	Assigned molecule ion in MS^2	Rel. peak areas [%] of the metabolite	
										ratHEP[b]	huHEP[b]
M_H16	6.67	B′	$[(C_{20}H_{23}F_3N_6O_3)Na]^+$ $[(C_{20}H_{23}F_3N_6O_3)H]^+$	475.1681 453.1856	475.1648 453.1894	−6.945 +8.385	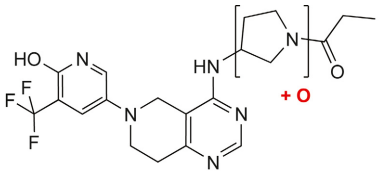	435.1762 379.1458 312.1073 245.1363 189.1074 172.0854	$[C_{20}H_{22}F_3N_6O_2]^+$ $[C_{17}H_{18}F_3N_6O]^+$ $[C_{13}H_{13}F_3N_6O]^+$ $[C_{10}H_{13}N_4]^+$ $[C_{10}H_{10}N_3]^+$ $[C_{10}H_{10}N_3]^+$	7.26	4.34
M_H21	15.7	D′	$[(C_{21}H_{27}F_3N_6O_3)H]^+$	469.2169	469.2175	+1.279	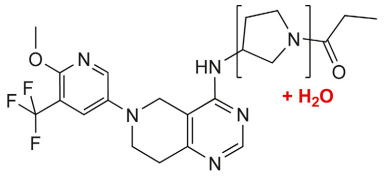	326.1227 265.1701 236.1418 192.1028 122.0704	$[C_{14}H_{15}F_3N_5O]^+$ $[C_{13}H_{21}N_4O_2]^+$ $[C_{11}H_{18}N_5O]^+$ $[C_{10}H_{14}N_2O]^+$ $[C_6H_8N_3]^+$	3.28	< 1
M_H25[a]	19.8	Y′	$[(C_{21}H_{23}F_3N_6O_2)H]^+$	449.1907	449.1905	−0.445	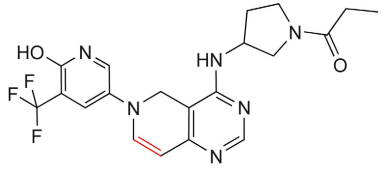	393.1650 376.1410 348.1068 324.1066	$[C_{18}H_{20}F_3N_6O]^+$ $[C_{18}H_{17}F_3N_5O]^+$ $[C_{16}H_{13}F_3N_5O]^+$ $[C_{14}H_{13}F_3N_5O]^+$	< 1	< 1
M_H34	5.4	E′	$[(C_{20}H_{23}F_3N_6O_4)H]^+$	469.1806	469.1826	4.263	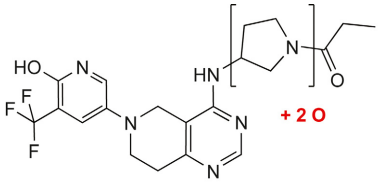	440.2942 335.1058 283.0714 279.1473 223.1182	$[C_{18}H_{19}F_3N_6O_4]^+$ $[C_{15}H_{12}F_3N_5O_3]^+$ $[C_{12}H_8F_3N_3O_2]^+$ $[C_{13}H_{19}N_4O_3]^+$ $[C_{10}H_{15}N_4O_2]^+$	< 1	2.93

[a] Confirmed by co-injection with synthetic reference. [b] Co-elution of $M_{HEP}3$ and $M_{HEP}10$.

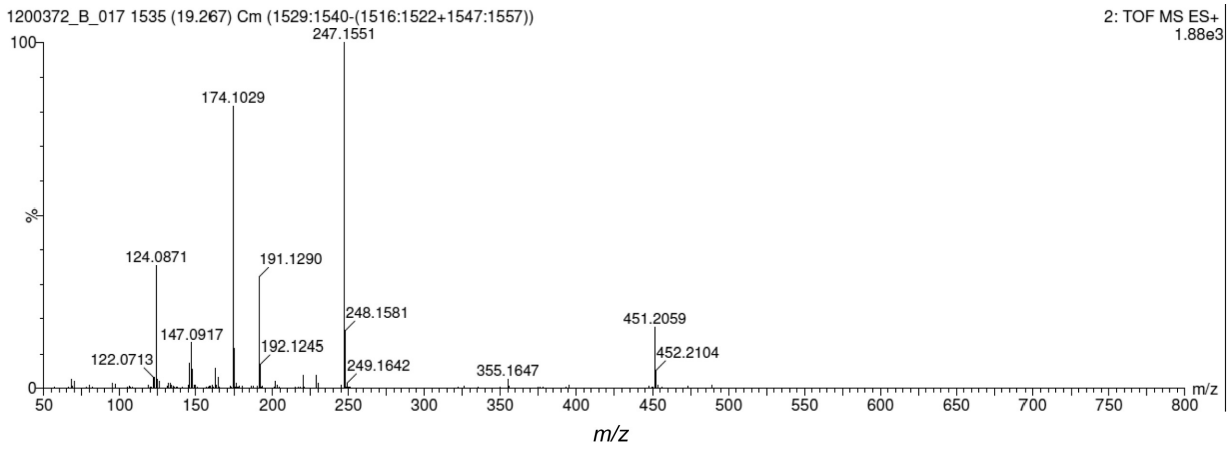

Figure 3. Q-TOF electrospray ionization MS/MS-spectra of CDZ173.

ammonia gives the tautomers of *m/z* 174.10. Upon loss of *m/z* 27 (probabely as $[C_2H_3]^+$), the distonoid ion *m/z* 147.09 seems to be formed, which – due to its reactivity – gives rise to slightly smeared (noisy) fragment patterns in this spectral region. This is expressed by losing formally C_2H_4 in order to form *m/z* 122.07 and a reduced species *m/z* 124.09.

Similar to the metabolite observed in microsomes (M_M), the hepatocyte metabolites (M_H) can be chategoterized into the groups A′ – E′. For structures and possible fragment interpretation of the metabolites discussed in this paragraph, see *Supplementary Material 1.3*.

Group A′ Metabolites: Metabolite M_H1. A precise $[M + H]^+$ (+ 0.655 ppm) was detected for the (hydrolytic) demethylation metabolite M_H1. Therefore it can be hypothesized that both metabolites M_M1 and M_H1 are identical. Further, that this metabolite is an integral part of metabolism in microsomes and hepatocytes. Practically, the identity was confirmed by coinjection with independently synthesized material (see below). Interestingly, in hepatocyte incubates, a hydrolysis product corresponding to M_M2 was not found.

Group B′ Metabolites: Pyrrolidine-mono-hydroxylation Metabolites M_H6, M_H7, M_H14, M_H16. The common fragmentation motive of the B′-group metabolites M_H6, M_H7, M_H14, and M_H16 are very similar to the key fragments postulated for the rDA process in CDZ173 (blue in *Scheme 2*). Compared to the parent's fragments (*Scheme 2*), the key fragments of these metabolites *m/z* 245.15, 189.11, and 172.08 are dehydrogenated, *i.e.*, contain an additional double bond compared to the parents fragment. Together with the well-defined $[M + H]^+$ of these metabolites (see *Table 4*), this additional double bond is a strong argument to narrow down the position of the hydroxyls to the pyrrolidine moiety. The fundamental difference between M_H6, M_H7 and M_H14, M_H16 though is that the first pair contains a O-methyl-group, while the second pair does not. Compared to the microsomal metabolites of group B (*Table 1*), four metabolites from hepatocyte incubation were clearly identified where *i*) a $[M + H]^+$ was detected and *ii*) the site of hyroxylation can be narrowed down with sufficient confidence to the pyrrolidine ring. Few O-demethylated metabolites were detected in microsomes. It must be noted, that in hepatocyte incubations no M_M17-like bioconjugate was detected which is a further argument that M_M17 is an assay artefact. In this context, it is likely that dehydrogenated ion peaks detected earlier for M_M11 and M_M25 in CID-MS/MS^n data (*Table 1* and *Table S1*) indeed are ionization artefacts, *i.e.*, it is justified to keep M_M11 and M_M25 in group B of the microsomal metabolites. Consequently M_H6 and M_H7 in group B′ correspond to the precursor of M_M11 and M_M25 in group B, *i.e.*, very likely M_M11 and M_M25 were spectral artefacts due to in source fragmentation of H_2O.

Group C′ Metabolite: N*-Propionyl-pyrrolidine Mono-Hydroxylation Metabolite M_H10.* Comparing the fragmentation pattern of M_H10 with the fragmentation pattern of B′-group metabolites reveals that characteristic ion fragments of M_H10 are not dehydrogenated, *i.e.*, *m/z* 191.12 and 174.10 are found. Since a $[M + H]^+$ was well defined in M_H10 while no fragment dehydrogenation was observed, the hydroxy group of M_H10 must be located in the propionyl side chain. Therefore, M_H10 in group C′ corresponds structurally to one of the three metabolites in the microsomal group C. Dehydrated forms of mono-hydroxylated M_H corresponding to M_M25 and

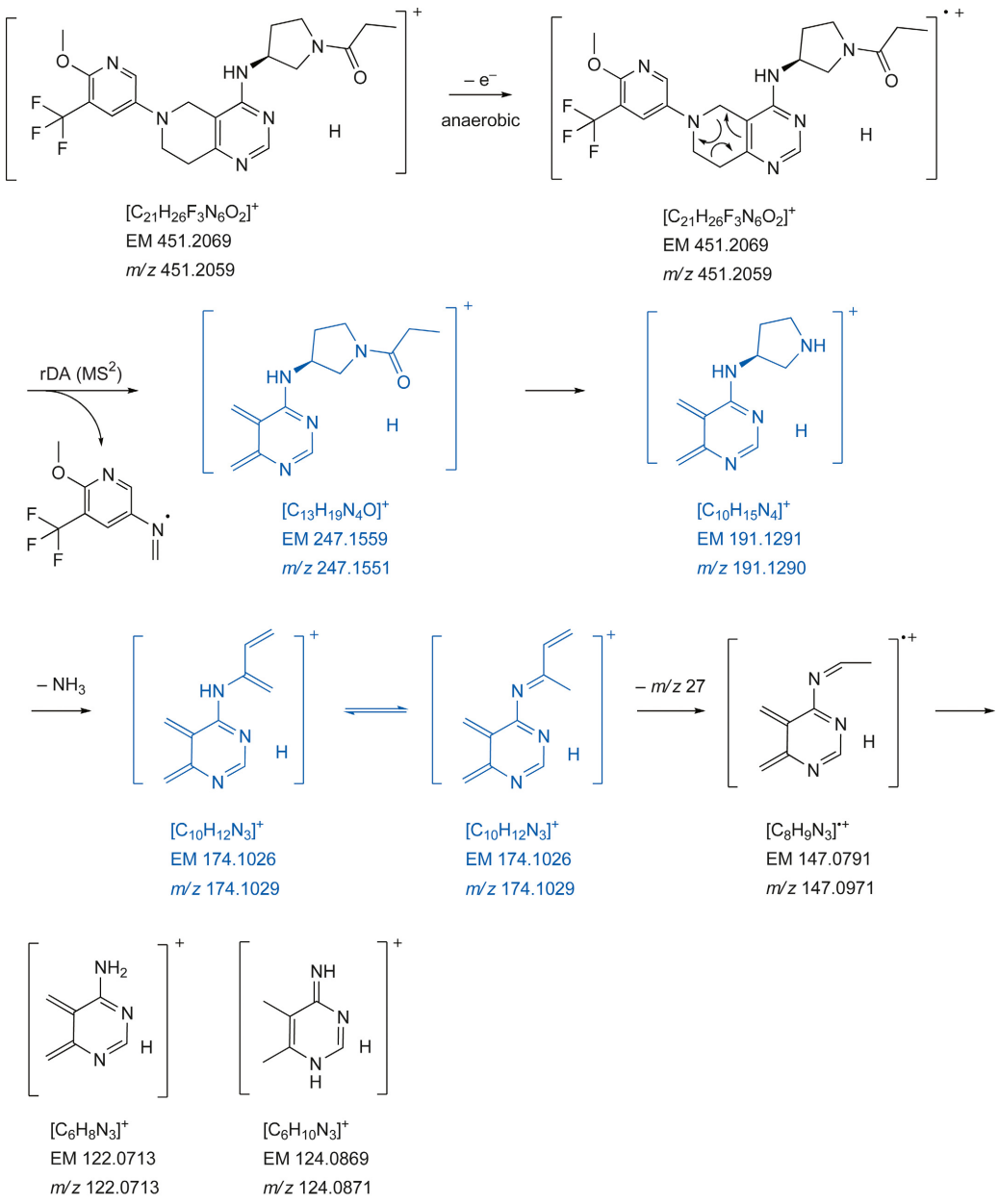

Scheme 2. ESI-MS/MS^n retro-*Diels–Alder* fragmentation hypothesis of unlabeled CDZ173. Structural key fragments observed in metabolites of CDZ173 are highlighted in blue.

conjugates corresponding to M_M17 (*Table 1*) were not found in hepatocytes.

Group D′ Metabolites: Formally Hydrated Metabolites M_H4 and M_H21. For M_H4 and M_H21, very precise $[M + H]^+$ at *m/z* 469.2169 and 469.2175 were observed (±0 ppm in the case of M_H4, +1.279 ppm in the case of M_H21. Both metabolites have very similar fragmentation patterns with characteristic fragments *m/z* 265.1633 (M_H4) and *m/z* 265.1701 (M_H21), which formally corresponds to a hydrate of the CDZ-key fragment *m/z* 247.15, followed by ring opening and reduction. In both cases, the characteristic cations *m/z* 326.1194 and 326.1227 in MS^2 were found. This finding narrows down the site of a C–N bond cleavage to the pyrrolidine moiety, however at this point it is not possible to distinguish which ring opening isomer is formed. Due to pyrroldine ring opening, *m/z* 265.1633 (M_H4) and *m/z* 265.1701 (M_H21) fragment differently than the corresponding key fragment of CDZ173 (*Scheme 2*). Upon formal elimination of propionamide, *m/z* 192.1 was found. According to the nitrogen rule, this exact fragment mass only is possible, when an impair number of

nitrogen atoms is present, *i.e.*, the cations at *m/z* 192.1 must contain oxygen. However, at this point two fragmentation solutions for these MS data are possible (see *Supplementary Material*), and thus it is impossible to distinguish by MS which pyrroldine ring opening isomers are formed (principally, ring opening is possible either *via* the N–C(2) or *via* the N–C(5) bond, while transamidation of propionyl to OH is chemically very unlikely; see *Table 1* for isomeric possibilities of these aminoalcohols). Based on the significantly different retention times of the discussed metabolites, it can be conclude that $M_H4 \equiv M_M4$ and $M_H21 \equiv M_M21$.

Group E′ Metabolites: Formal Pyrrolidine-bis-hydroxylation Metabolites M_H3, M_H5, and M_H34. M_H3 shows $[M + H]^+ = 483.1965$. Formally, for M_H3, a $(OH)_2$-analogon of the key fragment *m/z* 247.15 was found (*m/z* 279.1433). Further fragmentation yielded a vinyl at *m/z* 160.0869 as final fragment (*i.e.*, a fragment which contains one methylene less than the key-fragment *m/z* 174.1 in *Scheme 2*). Precursors for *m/z* 160.0869 are the fragments *m/z* 206.0928 and 364.1476. Since the difference of *m/z* 160.0869 and 206.0928 is 46.0059, it is reasonable to postulate the loss of CH_2O_2 in this step (EM = 46.0055). This indicates that *i*) *m/z* 206.0928 can be a cyclopropane with carboxyl substitution, in which the carboxyl substituent originates from the 2′-carbon of pyrroldine, *ii*) the C_3 moiety originates from C(3′), C(4′) and C(5′), and *iii*) initial geminal bis-hydroxylation ending in ring opening occurs on C(2′) (for structure proposal see *Supplementary Material 1.3*). In this context, it must be noted that *m/z* 244.1433 was not observed in other MS studies[27] with [^{14}C]CDZ173, *i.e.*, it is very likely an artefact. On the other side, M_H5 also exhibits a very intense *m/z* 483.1974 for its formal $(OH)_2$-analogon, which either can be a geminal bis-hydroxy on the same carbon (*e.g.*, on C(5′) of pyrrolidine) or the corresponding C(5′)-acid upon ring opening. *m/z* 483.1974 fragments into the depropionlyated rDA key fragments of its parent (*Scheme 2*) to yield *m/z* 279.1431 (= *m/z* 247 + *m/z* 32). Compared to M_H3, *m/z* 279.1431 of M_H5 fragments in a series of homologs (– *m/z* 29, – *m/z* 36, – *m/z* 36). Similar homologs are observed in the ESI of β-alanine and 1-propionic acid.[28] We interpret this difference in fragmentation as an argument that M_H5 is the corresponding C(2′)-acid with pyrrolidine ring opening. To conclude, M_H3 and $M_H5 \triangleq M_M3$ and M_M15 in the microsomal incubation (differences in retention time of M_H15 and M_M15 are explained since different HPLC hardware was used in these incubations). In the physiological context we are proposing for M_H3 and M_H15 the structures as shown in *Table 4*.

In the case of M_H34, the situation is different because *per se* the metabolite is O-demethylated. Nevertheless the rDA-key fragments at *m/z* 279.1473 ($(OH)_2$-analogon together with a reduced species as observed for CDZ173) and at *m/z* 223.1182 ($(OH)_2$-analgon of *m/z* 191.12 found for CDZ173; *Scheme 2*) were found in MS^2. Based on this finding the exact site of oxidation of the pyrrolidine ring is not clear.

Group X′ Metabolite: N-Oxide M_H9. M_H9 is an previously not detected N-oxide $[M + H]^+$ at *m/z* 467.2018 (±0 ppm). M_H9 shows the same fragments *m/z* 324.1045, and *m/z* 263.1514 as detected for the synthetic reference **20** (see *Experimental Section*), however the characteristic H_2NO-elimination fragment (radical cation $[M]^{\cdot+}$ at *m/z* 435.1817) is better seen in + ESI MS^2 of **20** (see *Supplementary Material*). This characteristic fragment defines the oxygen to be located at N(1) of the pyrimidine. rDA-fragmentation of M_H9 yields the O-adduct of the characteristic key fragment *m/z* 247.15 at *m/z* 263.1514. In case of M_H9, a fragmentation competing with the rDA model is observed. This is seen in the fragment *m/z* 324.1045, in which $[M + H]^+$ losses the pyrollidine moiety and formally eliminates H_2O.

Group Y′ Metabolite: THP-Dehydrogenated Metabolite M_H25. M_H25 exhibits at characteristic $[M + H]^+$ at *m/z* 449.1905, which proves the presence of an additional double bond equivalent compared to the parent. Therefore, rDA process in the THP moiety cannot be observed. Instead M_H25 loses propionyl. The pyrrolidine ring eliminates NH_3 (– *m/z* 17) to form butyl and acetylen fragments (*m/z* 376.1410 and 348.1068). In parallel, M_H25 was prepared synthetically (compound **21**, *Experimental Section*) to further characterize M_H25. M_H25 may not be confused with the microsomal metabolite M_M25, where the double bond is located in the pyrrolidine moiety ($M_H25 \neq M_M25$).

Structure Confirmation of M_H1, M_H9, and M_H25 by Co-Injection with Synthetic References. To unambiguously confirm the structure of M_H1, M_H9, and M_H25, the synthetic references **19** (M_H1), **20** (M_H9), and **21** (M_H25) were synthesized (see *Figure 4* for structures). The O-demethylated product **19** and the pyrimidine-*N*-oxide **20** were accessible by incubation of CDZ173 with the soil micro-organisms *S. platensis* and *S. griseus*, respectively (see *Experimental Section* for details). Facing the low one-electron oxidation-potential of TMPD compared to the oxidation

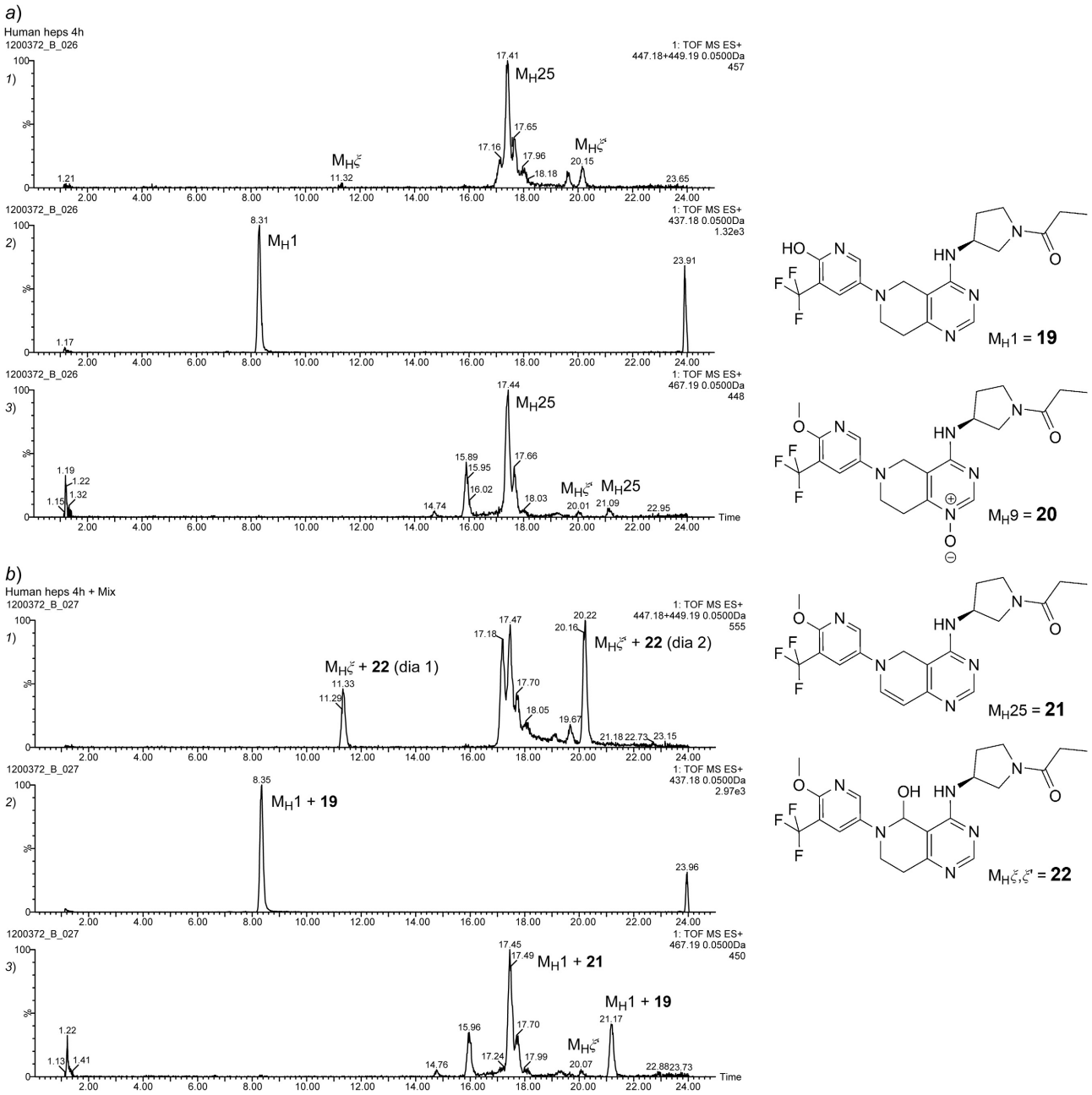

Figure 4. *a*) Radio-LC/MS traces of the incubation of CDZ173 with huHEP after 4 h. *1*) LC/MS at 447.18 – 449.19 Da. *2*) LC/MS at 437.18 Da. *3*) LC/MS trace at 467.19 Da. *b*) LC/MS of A at the same mass points *1*), *2*), and *3*) after adding a 1:1:1:1 mixture of **19**, **20**, **21**, and **22**.

potential of 4-amino-pyrimidine, the selectivity in this aerobic biotransformation process is surprising. **20** was characterized by $^{+}$ESI-MS/MS showing the expected radical cation $[M]^{\cdot+}$ at *m/z* 435.1817 (see *Supplementary Material*) and by comparing the ^{13}C-spectra of **20** with the ^{13}C-NMR of CDZ173. There a high field shift for C(2″) in **20** compared to C(2″) in CDZ173 was observed (147.6 ppm in **20** *vs.* 155.8 ppm in CDZ173). Compared to the signal for C (8d″) in CDZ173 (δ(C) = 158.8 ppm; see *Experimental Section* for C-atom numbering in CDZ173), the signal of C(8d″) in **20** was shifted high field (δ (C) = 150.1 ppm). Compound **21** – the synthetic reference for M_H25 – was obtained as a mixture with the two diastero-isomers of **22** by oxidation of CDZ173 with laccase from *Trametes versicolor*. To confirm the structures of M_H1, M_H9, and M_H25, a diluted mixture of **19** – **22** was prepared and co-injected with incubates from huHEP and ratHEP after 4 h incubation time. *Figure 4* shows the LC/MS traces

at different mass points. It can be seen, that after co-injection M_H1 (t_R = 8.31), M_H9 (t_R = 2.09), M_H25 (t_R = 7.44) and two diasteroisomers of a previously not identified hepatic metabolites $M_H\xi$ and $M_H\xi'$ (t_R = 11.32 and t_R = 20.15) came up. Based on this co-injection it is proven that $M_H1 \equiv$ **19**, $M_H9 \equiv$ **20**, $M_H25 \equiv$ **21**, and $M_H\xi$,$M_H\xi' \equiv$ (3′*S*,5″-*rac*)-**22**.

Metabolic Pathway. Based on the data presented above, we were able to outline a hepatic metabolism pathway based on metabolites formed *in vitro* in hepatocytes (*Scheme 3*). The key metabolic pathways were oxidative, involving predominantly O-demethylation (*e.g.*, M1) and pyrrolidine hydroxylation (*e.g.*, M6, M7) as well as several minor oxidative pathways. Similar metabolites were identified to those found in the qualitative microsomal metabolism investigation (*Table 1*) except that the THP oxidation pathway was not identified in the hepatocyte experiment. Additionally, no phase II metabolites were identified in hepatocytes. These differences could be assigned to differences in metabolic pathways between microsomes and hepatocytes; however, as the hepatocyte study was performed quantitatively with a tritium radiolabel and the microsome study was qualitative, it is also feasible that the additional microsomal metabolites are simply

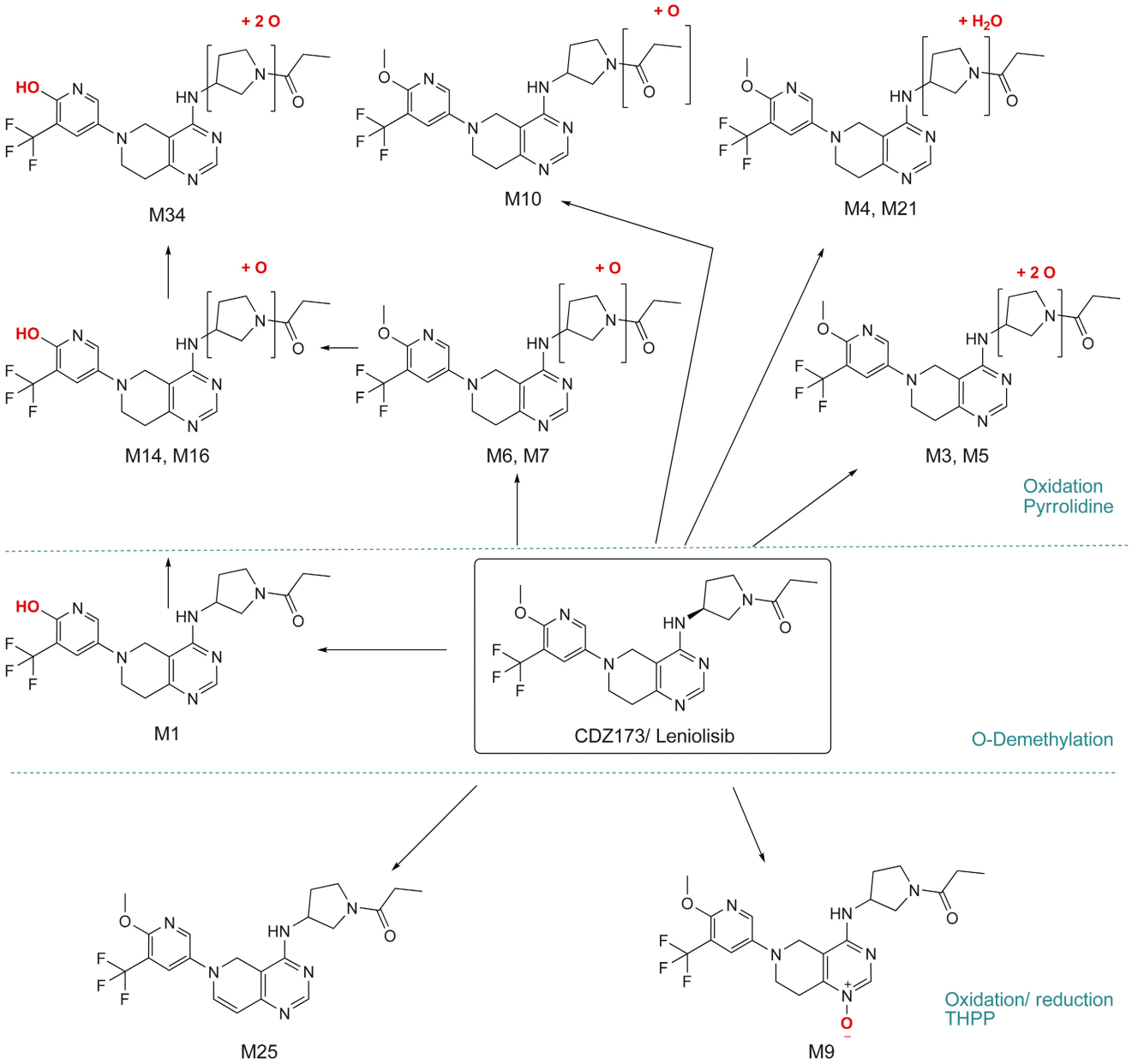

Scheme 3. Metabolic pathway of CDZ173 as concluded from MS/MS^n data acquired in this study.

quantitatively minor and therefore not detected in hepatocyte experiment. This hypothesis is supported by *in vivo* data showing that THP oxidation metabolites are formed but at low abundance.[27] The next project steps, *i.e.*, identifying the cytochrome complexes responsible for the biotransformation to the discussed metabolites were not covered by the project plan at the time of approval, but might be addressed at a suitable point elsewhere.

NMR of CDZ173

NMR of CDZ173 and its synthetic metabolite references **19** – **22** was hampered due the dynamics of the amide bond causing *pseudo*-rotamers and different conformations of the pyrrolidine ring. In this paragraph, we focus on the NMR discussion of the common parent. Our model to understand the 2D-NMR spectra of CDZ173 takes into account the rotational barrier of the amide bond of *N*-trifluoroacetyl pyrroldine. The activation barrier for *cis-trans* isomerism for this compound was found to be $\Delta G_{298}^{\ddagger} = 80.4$ kJmol^{-1} in solution and $\Delta G_{298}^{\ddagger} = 71.4$ kJmol^{-1} in the gas phase, while the pseudorotational barrier in pyrrolidine was calculated to be 0.6 kJmol^{-1} *ab initio* taking into account that the nitrogen inversion of the pyrrolidine ring is of little importance in *N*-trifluoroacetyl pyrrolidine.[29][30] On the other side, we consider the *ab initio* conformational analysis of *Reiher* and *Seebach* on C(2′)-substituted pyrroldines, where the pyrrolidine nitrogen is bound to a sp^2-hydridized carbon.[31] These authors calculated that UP- and DOWN ring conformers of pyrrolidine are both significantly populated when a *Boltzmann* distribution is in equilibrium. Similar to what is known for solubilized poly-Pro-peptides[32][33] one must assume *cis*- and *trans*-isomerism along the dihedral angle C(2)–C(=O)–N–C(2′) in combination with UP/DOWN conformers of the pyrroldine ring (see *Experimental Section* for a C-atom-numbering in CDZ173 consistent with rules of nomenclature). *Scheme 4* shows this situation together with the characteristic NOE signals to be expected. The dihedral angle C(2)–C(=O)–N–C(2′) is high-lighted in red. For reasons of graphic clarity the flat pyrimidalization of nitrogen is neglected.

NMR Spectra of CDZ173 showed that two distinct structures are present in a 1:1 ratio at room temperature in (D$_6$)DMSO which were assigned to be conformers as illustrated in *Scheme 4*. In case of CDZ173 and its synthetic metabolites and precursors, chemical homongenity was proven by HPLC and in case of the synthetic precursor (*S*)-**8** (*Scheme 1*) also by high temperature NMR. At 373 K, a single structrue was observed for (*S*)-**8**. For this reason, it is justified to anticipate the same conformational colascence behavior for CDZ173 and its derivatives.

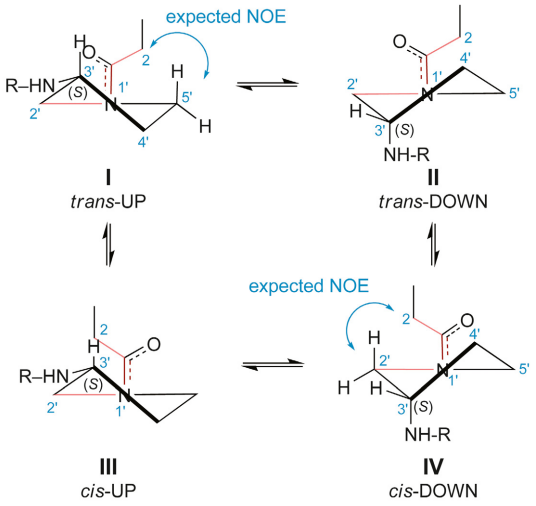

Scheme 4. *cis/trans - UP/DOWN* conformational isomerism in CDZ173 and its derivatives.

The existence of two conformers of CDZ173 at 298 K was seen in the ^{1}H-NMR, *e.g.* in CDZ173, where H–C(3′) of the (*S*)-amino functionality in the pyrrolidine gave two well resolved *sextets* at 4.70 ppm (^3J = 6.6 Hz) and 4.58 ppm (^3J = 6.4 Hz). Complete ^{1}H- and ^{13}C-signal assignment with open diastereotopicity was achieved from COSY, TOCSY, HSQC, and HMBC-data. COSY-, TOCSY-, HSQC-, and HMBC-signal assignment using standard semi-automated assignment tools has shown that NOE peaks exist, which were interpreted as signals between the CH$_2$-group of the propionly side chain and either of the two amide-vicinal CH$_2$-groups of the pyrrolidine conformers (*Figure 5*). Key to the differentiation between H110 and H111 of one conformer and H53 and H54 of the second conformer were distinct TOCSY, HSQC- and HMBC-signals for these protons in both conformers.

Although noise was found in the f2-dimension of the ROESY-spectra, the observed NOE correlations are consistent with the validated assignment obtained from the data set mentioned above, *i.e.*, for the first conformer (highlight green in *Figure 5*) qualitative cross-peak correlations between CH$_2$-propionly (protons 53 and 54 in *Figure 5*) and the CH$_2$(2′) group of the pyrrolidine moiety (protons 46 and 47 in *Figure 5*) were found defining the constitution of the amide bond in CDZ173 *trans* to the amino group in the pyrrolidine ring. Based on the hypothesis outlined in *Scheme 4, a trans*-amide bond with cross peaks to only one side of the pyrrolidine requires an UP-conformation of the pyrrolidine. In this conformation, the oxygen is *cis* to the substituent on C(3′).

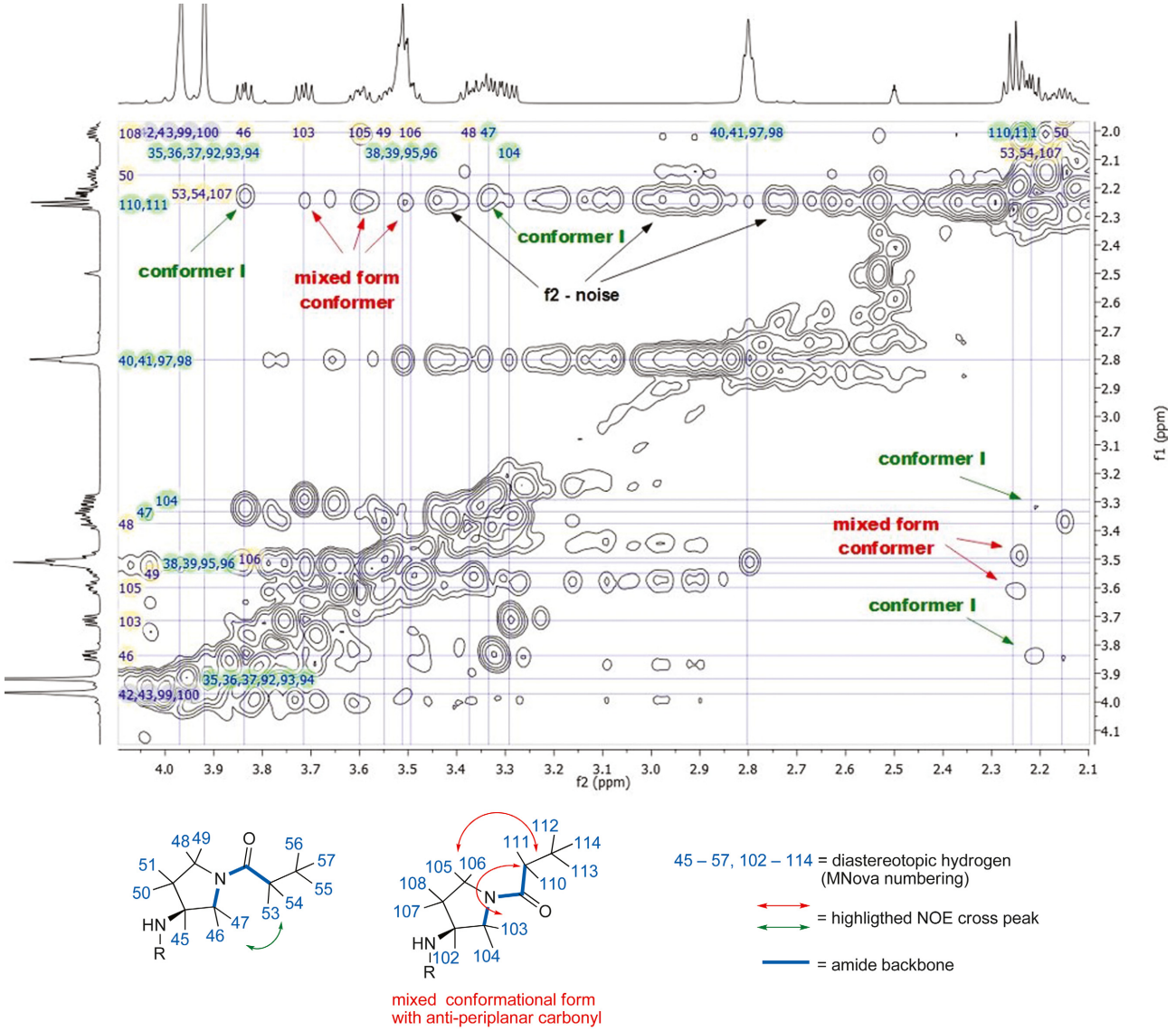

Figure 5. ROESY-spectra of CDZ173 in the cross peak region of CH_2-propionyl and the amide-vicinal CH_2-groups of the pyrrolidine (600 MHz, 25 °C, Gaussian denoised and smoothened, semi-automated assignment with MNova v11.06).

In our data, these cross-peak correlations are slightly, but distinctively high field shifted. Consequently, the intense signals which are standing out from the fading f2-noise line (*e.g.* cross peak 110/111 ↔ 105 in the upper half of the spectrum) were interpreted as NOE correlations of the second conformation (red in *Figure 5*). Reflected cross peaks for this conformer without noise were found in the lower triangle of the spectra. Since cross peaks between hydrogen 110/111 and the hydrogens 103 and 105/106 are observed, a qualitative solution conformation is very likely, in which the propionly side chain stands anti-periplanar to the pyrrolidine ring and the carbonyl-oxygen must point out of plane of the pyrroldine, *i.e.* a mixed conformational form between a cis and trans amide bond is present. This means that the pyrrolidine ring in this conformation of CDZ173 must be relatively flat compared to the conformer discussed above.

This qualitative NMR-analysis shows that in (D_6)DMSO two conformers each with different pyrrolidine puckering similar to the proline puckering in peptides[34] have reached the energy minimum and are present in solution at room temperature. Further it means that the rotational barrier between both conformers must be at least 81 kJ/mol and slightly lower at body temperature so that one conformer binds to PI3Kδ. A similar conformational homogenization upon binding was observed in conformers of small molecule PRO-ligands upon binding to a cofactor.[35] For the

synthetic metabolites **19** – **22**, the same 1:1 ration was observed in the ^{1}H-NMR spectra, however a qualitative conformational analysis was not undertaken for these metabolites, *i.e.* analytical data of these conformers are reported as 'conformer A' and 'conformer B' in the *Experimental Section* In the biologically relevant X-ray structure of CDZ173 bound to PI3Kδ,[2][36] the backbone of CDZ173 is *cis*, the oxygen is neither *cis* nor *trans* relative to the axial C(3′) substituent and the pyrroldine puckering corresponds to the conformer IV in *Scheme 4*, while the carbonyl side chain is in plane with the pyrrolidine. To conclude, during the binding of solubilized CDZ173 to PI3Kδ, a conformational change of CDZ173 occurs *via* homogenisation towards a planar *cis* backbone and a DOWN-puckering of the ring. In (D_6)DMSO, this situtation corresponds to the second conformer with δ(H) H–C(3′) = 4.58 ppm. From such a conformer the energy minimun seen in the biological X-ray structure must be reached most easily.

Summary, Conclusions and Outlook for ^{3}H-Labelling Strategies

During this project, a first metabolic landscape based on ESI was created. Extensive metabolism was observed; however the pyridine moiety of CDZ173 remained chemically inert. Based on these data, a synthetic target of a metabolically stable tritium tracer of CDZ173 ([^{3}H]CDZ173, **1b**) was designed and developed yielding several batches of enantiomerically pure [^{3}H]CDZ173 with a specific activity of 600 GBq/μmol and radiochemical purity > 98% HPLC. In a diluted formulation [^{3}H]CDZ173 was incubated with human and rat hepatocytes and the incubates were analyzed by high resolution ESI tandem MS. During the validation of [^{3}H]CDZ173, no tritated water was observed qualifying this tracer as a tool to study liver metabolites. Consequently, this ^{3}H labelled tracer is suitable for use in preclinical and potentially clinical ADME studies once the cytochrome C enzymes are identified responsible for the biotransformations. Hence, the hypothesis postulated by *Krauser*[7] that ^{3}H-labelling is a sophisticated and cost effective tool to *i*) replace expensive ^{14}C-multi step labelling and *ii*) to study ADME properties of modern pharmaceuticals was proven experimentally. Compared to tritium labels commonly prepared by catalytic hydrogen-isotope exchange methods yielding more or less a random and difficult to predict distribution of tritium in the most reactive positions of the molecule, non-radioactive organic synthesis combined with microsome screening and structure elucidation appears to be the tool of choice to provide a safe precursor, which is ready for tritiation in a metabolically stable position at a time when the pharmaceutical compound still is in phase 0. Nevertheless, following a standard operating protocol (SOP) of the isotope lab unit, every tritiation candidate was tested for hydrogen isotope exchange using the Crabtree catalyst (typical procedure is first max. 5 mol-% *Crabtree* catalyst loading in CH_2Cl_2 with $p(D_2)$ = 1 atm using the balloon technique for gas transfer, then up to equimolar amounts of catalyst under the same conditions). The synergetic purpose of this SOP is to test the general chemical reactivity towards transition metal insertion, hence the possibility of metabolic loss of the label as it occurs in cytochrome c enzyme by the iron cofactors. When this SOP conditions were applied to CDZ173, no significant mass change was detected by LC/MS. Under the SOP conditions no exchange was observed in the methyl of the esterified 2-pyrollidon moiety of CDZ173 as it was it was mentioned in the scientific literature[37] and reproduced with high specific activity by *Crabtree*-exchange for the structurally related orexin 2 receptor EMBA by the first author.[38] In case of CDZ173, we assign this finding to the presence of an electronic withdrawing CF_3-group in CDZ173 compared to EMBA, where this particular Ir-catalyzed exchange must follow an unorthodox exchange mechanism. However, even if this Ir-catalyzed exchange reaction was successful in the OCH_3-group of CDZ173, the label would have been lost during tracer application (see *Table 1*, group A metabolites).

After the development of the tritium label for this project was completed, a pincer-type, oxygen sensitive iron-catalyst was applied by the *Chirik* group in 2016 for the labelling of structurally relevant model compounds (*e.g.* compounds 12 and 17 in figure 2 in the discussed publication) and the application of this catalyst for the hydrogen isotope exchange of *e.g.* the *Merck* compounds *MK-7246* and *MK-8228* as well as to the *Amgen* compound *Cinacalcet* (figure 3 in the discussed publication).[39] In case of *MK-7246*, exchange was observed in an aromatic *ortho, ortho′* position of a fluoro-benzene. In case of *Cinaclacet* and *MK-8228*, exchange occurred in the *meta*-position of CF_3-phenyl and the *meta*-position of MeO–phenyl. Unfortunately, the *Chirik* catalyst is chemically stable in C_6D_6 for 1 day only.[40] Generally seen, the authors applied this exchange technology to aromatic compounds with a lower degree of substitution in the exchanging benzene ring. To which extend the mainly di-substituted substituents of the application molecules can be compared with the substitution pattern of the pyridine in CDZ173 is unclear. In any case, relevant pyridine

positions in CDZ173 are occupied or sterically hindered. Consequently it remains to be tested if the carbene-iron complex indeed can exchange in the electronically and sterically challenging positions H–C(6) of the pyridine in CDZ173.

In this context, it must be emphasized that our microsome and hepatocyte incubations, which certainly hydroxylate CDZ173 based on cytochrome P450, non-heme diiron hydroxylases and α-keto-glutarate dependent non-heme iron hydroxylases following an oxygen rebound mechanism[41] are incompatible with the mechanism proposed for a *Crabtree*-type catalyst. If α-keto-glutarate dependent non-heme iron halogenases following a non-oxygen rebound mechanism are present in our assays is not addressed. To the best of our knowledge the last-named enzyme class plays a minor role in liver metabolism. On the other side cytochrome c3 and cytochrome c6, which both have hydrogenase activity under certain conditions[42] are indeed relevant *e.g.* in the liver metabolism of taxol.[43] To which extend [FeFe]-hydrogenase cluster exchange in H–C(6) of the pyridine and therefore are a mechanistic model for the *Chirik* catalyst is unclear. This argumentation further supports the experiment suggested with this catalyst.

To conclude, our synthetic approach at the time when the tritium-synthesis was developed is defined by nature and bio-analytics rather than *ab initio* manual screening of catalysts in order to achieve the goal. Of course, in this context it must be noted, that analytical assays are known to accelerate catalyst screening (*e.g.* ref. [44]). Seen from an economic point of view, it must be evaluated at which point in the pharmaceutical development process bigger resources shall be spent on automated exchange catalyst screening. Only future basic research can show to which extend the hydrogenase activity in a hepatocyte incubation assay of a pharmacophore run under 95% air and 5% CO_2 in aqueous buffer (see *Experimental Section*) can predict if a synthetic catalyst, which – ideally – should be identified at least for every lead structure of a med-chem library, can be applied successfully. Achieving this goal would certainly raise the practicability of the hydrogen-isotope technology in case of some clinical candidates.

Experimental Section

Incubation with Liver Microsomes and Sample Preparation from Bile Cannulated rat and LC/MS^n Analytical Method

In vitro *Incubations.* Incubations (0.5 mL each) were performed at 37 °C in a shaking incubator. The incubations contained rat, mouse, dog, monkey, and human liver microsomes at a protein concentration of 0.3 mg/mL in 0.1 M KH_2PO_4 buffer (pH 7.4), CDZ173 (5 μM) and $MgCl_2$ (5 mM). The mixture was pre-incubated for 3 min at 37 °C before addition of GSH (1.5 mM), alamethicin (1.25 μM), UDPGA (2.4 mM), and an NADPH regenerating system containing isocitrate-dehydrogenase (1 U/mL), NADP (1 mM), isocitrate (5 mM). Reactions were stopped after 1 h by addition of an equal volume of ice-cold MeCN. The samples were then vortex-mixed and centrifuged for 5 min at 10000 g. 0.1 mL of supernatant was diluted with 0.4 mL water and filtered (*Ultrafree MC* filters, *Durapore PVDF*, 0.45 μm, *Millipore*). The resulting supernatants were transferred to a clean autosampler vials for LC/MS^n analysis.

In vivo *Experiments Using Bile Duct Cannulated Sprague–Dawley Rats. White coat Sprague Dawley* male rats (Crl:CD (SD), 320 g) were used and were obtained from *Charles River Laboratories* (*Iffa-Credo*, France). The *in vivo* experiment was performed according to the regulations effective in the Canton Basel-City, Switzerland, specifically according to experimental license No. 2241. The study was performed as described previously.[45] Briefly, the *Sprague–Dawley* male rat as specified in the general experimental part was used for this study. The day before drug administration, the animal was anaesthetized and then, under aseptic conditions, three catheters were successively implanted and fixed into its femoral artery, femoral vein, and bile duct for blood collection, drug administration, and continuous bile collection, respectively. The animals were allowed to recover for 24 h following surgery. The duration of the study was 8 h, throughout which, the animal was housed in a metabolic cage. CDZ173 (3 mg/kg, 0.5 mL/kg a solution in NMP/PEG, 30:70, v/v) was administered intravenously *via* the femoral vein catheter. Bile was collected for up to 8 h post-dose at pre-defined time intervals (0 – 2 h, 2 – 4 h, 4 – 6 h, 6 – 8 h) while sufficient urine was only obtained during 4 – 6 h. Blood samples were collected at 1, 4, and 8 h post-dose. All samples were collected on ice, then frozen as soon as possible at −80 °C until analysis.

Preparation of in vivo *Samples for LC/MS^n.* Bile and urine samples were thawed, centrifuged, and pooled from each time intervals and diluted with H_2O/MeCN (9:1). The diluted samples were then filtered to remove any precipitated material. Blood samples (0.1 mL) were treated with 0.3 mL ice-cold MeCN, thoroughly mixed and then centrifuged (10 000 *g*, 5 min). A volume of 0.4 mL of the supernatant was

transferred to a new vial and concentrated using a *Cyclone* high speed evaporator. The residue was then reconstituted with 0.25 mL H_2O/MeCN (9:1) and filtered. The resulting supernatants were transferred to clean autosampler vials for LC/MS^n analysis.

LC/MS^n Analytical Method. Capillary HPLC was performed using a *Chorus-220* HPLC pump (*CTC Analytics*, Switzerland), a *HotDog-5090* column oven (*Prolab*, Switzerland) and a *HTS-PAL* or an *LC-PAL* autosampler with cooled sample stacks (*CTC Analytics*, Switzerland). Chromatographic separations were performed using a *Reprosil Basic HD C18* capillary HPLC column (3.0 μm, 0.3 mm × 150 mm, *Morvay Analytik*, Basel, Switzerland) with a flow rate was 4.5 μL/min. The injection volume was 1 μL. Mobile phase *A* consisted of aqueous ammonium formate (10 mM, with 0.02% TFA, pH 6)/MeCN (95:5, v/v). Mobile phase *B* consisted of aqueous ammonium formate (10 mM, with 0.02% TFA, pH 6/MeCN/MeOH (5:90:5, v/v/v).Chromatographic separations used a linear solvent gradient: 0 min (5% *B*), 2 min (5% *B*), 25 min (95% *B*), and 32 min (95% *B*, 6.5 μL/min). Re-equilibration of the column was performed at 5% *B* for 5 min. The column temperature was maintained at 40 °C. Samples were stored at 10 °C in the autosampler until injection. The Capillary HPLC system was coupled to a *LTQ XL Ion Trap/Orbitrap* (*Thermo Scientific*, CA, USA) mass spectrometer equipped with an ESI source (*Thermo Scientific*, CA, USA) operating in positive mode with a source voltage of approximately 4 kV and a capillary temperature of 275 °C. Auxiliary and sheath gas flow rates (both 99% purity N_2) were 1 and 15 (arbitrary units), respectively, whereas sweep gas was not used. Mass spectral data were acquired in data-dependent mode with full-scan spectra obtained from *m/z* 150 – 1000 with a mass resolution of 30 000. CID data-dependent MS/MS scan events were carried out with normalized CE of 25 arbitrary units. MS^2 scan events were triggered for the two most intense ions and MS^3 scan events were triggered for the two most intense ions from each MS^2 scan. AGC target settings were 5×10^5 and 1×10^4 for full MS and MS/MS, respectively. The polysiloxane background ion $[C_2H_6SiO]_6$ with *m/z* 445.12003 was used as lock mass.

Synthesis and Radiosynthesis

General Abbreviations. AGC: Auto gain control, MeCN: acetonitrile, BINAP: (2,2′-bis(diphenylphosphino)-1,1′-binaphthyl), ^{t}BuMePhos: 2-(di-^{t}butylphosphino)-2′-methylbiphenyl, ^{t}BuOH: *tert*-butanol, CE: collision energy, CID: collision induced dissociation, CYH: cyclohexane, CH_2Cl_2: dichloromethane, DEA: diethanolamine, Et_2O: diethyl ether, DMSO: dimethyl sulfoxide, AcOEt: ethyl acetate, ETPH: ethyl-benzene, ESI: electrospray ionization, FA: formic acid, GSH: glutathione, HEP: heptane, HEX: hexane, AcOH: acetic acid, IPA: isopropylalcohol, i.v.: intravenous, LC/MS^n: liquid chromatography/multi-stage mass spectrometry, MeOH: methanol, MeONa: sodium methoxide, Me_4-^{t}BuPhos: di-*tert*-butyl(2′,4′,6′-triisopropyl-3,4,5,6-tetramethyl-[1,1′-biphenyl]-2-yl)phosphine, MOPS: 4-morpholinepropanesulfonic acid, NADP: nicotinamide-adenine-dinucleotide-phosphate, NMP: *N*-Methylpyrrolidone, Pd_2dba_3: Tris(dibenzylideneacetone)-dipalladium(0), PEG: polyethylenglycol, r.t.: room temperature, t_R: retention time, SD: *Sprague Dawley*, Et_3N: triethylamine, TFA: trifluoroacetic acid, TEMPO: (2,2,6,6-tetramethylpiperidin-1-yl)oxidantyl, UDPGA: uridine 5′-diphosphoglucuronic acid.

Biochemicals, Chemicals, and Reagents: Analytical Reagents. *CHROMASOLV® Plus* high-performance liquid chromatography (HPLC) grade (*Sigma*, Switzerland) or *HiPerSolv ChromaNorm* HPLC/MS grade (*VWR Chemicals*, France) water was further purified by distillation using a *Water Still Distinction D4000* (*GMB Glasmechanik*, Switzerland) and stored in plastic labware for usage on the capillary HPLC system. *CHROMASOLV®* HPLC grade acetonitrile (MeCN), HPLC grade methanol (MeOH), phosphate buffer (1.0 M pH 7.4), TFA was purchased from *Sigma* (Switzerland). Ammonium formate was purchased from *Fluka* (Switzerland). Nitrogen (purity 99.5%) and Argon (purity 99.995%) were purchased from *Carbagas* (Switzerland). Pooled rat, mouse, dog, cynomolgus monkey, and human liver microsomes were purchased from *BD Biosciences* (Woburn, MA). *Culture media NL148S*: 0.2% soluble starch (*Sigma*), 0.8% soya peptone (*Sigma*), 0.4% *Oxoid Lab-Lemco*, 0.05% yeast extract (*Sigma*), 0.15% NaCl, 0.21% MOPS, adjusted to pH 6.50 (1 N NaOH/1 N HCl), and trace element solution (1 mL/L). The trace element consisted out of $Na_2MoO_4 \cdot 2\ H_2O$ (30 mg/L), $FeSO_4 \cdot 7\ H_2O$ (5.5 g/L), $CuSO_4 \cdot 5\ H_2O$ (80 mg/L), $MnCl_2 \cdot 4\ H_2O$ (180 mg/L), $ZnSO_4 \cdot 7\ H_2O$ (4.4 g/L), and H_2SO_4 97% (2 mL/L). *Streptomyces platensis*: strain type 40041 (DSM). Preculture of *streptomyces griseus* (strain ATCC No. 55185) was grown in 100 mL NL148s medium in 500 mL shake flasks at 26 °C and 220 rpm for 3 days. *Nutrient solution*: 40 g/L glucose, 40 g/L lactose, 60 g/L sodium citrate dihydrate. The reference **1a** for the release analysis of **1b** was a registered sample from the *Novartis* compound archive. *McIllvaine buffer* pH 4.5: prepared according to.[46] *Reagents for small molecule organic synthesis*: All starting materials and

solvents were of common commercial origin (*Sigma*) and were used without further purification.

Special Equipment for Synthesis and Glassware for Non-Radioactive Synthesis. Only were explicitly stated, reactions were carried out in an inert atmosphere of nitrogen (99.5% purity). For the synthesis of **17**, *Schlenck* technique was applied for reaction and reagent transfer at low temperature.[47] Cooling bath temperature < −80 °C was achieved by adding liq N_2 to a MeOH bath. Microwave assisted synthesis was performed using *CEM Microwave Discover* apparatus ramping with 200 W to 110 °C. Automated flash chromatography: *ISCO* flash chromatography system or *Analogix Intelli Flash 280* with *Supel* flash cartridge, 40 – 63 μm, active silica bed.

Tritiation. Halogen–tritium exchange reactions were performed on a *316L* stainless steel, helium-leak tested vacuum manifold custom made by *RC Tritec AG*, CH-9053 Teufen. The getter technology used on this manifold is based on the thermal, reversible equilibrium of uranium(III) tritide, uranium and tritium according to 2 $^{238}UT_3 \leftrightharpoons 2\ ^{238}U + 3\ T_2$.[48][49] The manifold contains a depleted uranium reservoir with 185TBq T_2 per 15 g ^{238}U (forward reaction), a depleted uranium recycle flow reservoir (reverse reaction) and a waste ampule to recover contaminated solvents and organic volatiles. Tritium gas generated in the forward reaction is 99% pure with A_{spec} = 95.9 GBq/mL. Reactions on this manifold are performed at r.t. in 2 mm *Pyrex* glassware (2 mL two-neck-round-bottom flasks and 25 mL lyophilisation ampule each with 3/8″ cylindrical fitting). Tight connection of glassware is assured by using a Keel-F ferrule system. The manifold system contains integrated reservoir heating system for the reservoirs and pressure measurement systems in each compartment.

Hardware for Instrumental Analytics of Synthetic Compounds. For flash chromatography, in process TLC control, radio-detection of [^{3}H]CDZ173, determination of the specific activity by MS, open access LC/MS, and service-MS of intermediates and final products, the same hard ware equipment was used as described in detail in the experimental part of a publication from the isotope lab unit.[50] For GC-MS analytics of the bis-halogenated pyridines **16** – **18**, a *Waters GTC* GC/MS accurate mass instrument was used.

HPLC Methods for Analytics, Preparative Chromatography, and Release of Synthetic Compounds. HPLC-Method I (chiral analytical): *Gilson*. Enantiomer baseline separation on *Venusil* chiral *OD-H*, 4.6 × 250 mm, 5 μm, 25 °C, λ = 254 nm, flow 1 mL/min, P = 4.0 – 5.4 MPa, isocratic separation with 0.1% Et_3N in Hex/EtOH 90:10. *HPLC-Method II* (chiral preparative): *Gilson*. Enantiomer baseline separation on *Venusil* Chiral *OD-H* 211 × 250 mm, 5 μm, 25 °C, λ = 220 nm, 254 nm; mobile phases for gradient elution *A* = 0.2% DEA in Hex and *B* = 0.2% DEA in EtOH. *HPLC-Method III: Agilent 1100* Series. Column: *Waters Sunfire RP C18*, 19 × 250 mm, 5 μm, 25 °C, λ = 230 nm, flow 25 mL/min, mobile phases for gradient elution phase *A* = water and phase *B* = MeCN, gradient: 20 – 55% *B* (16 min), 55 – 95% *B* (1 min), 95% (2 min), 95 – 5% *B* (1 min), 20% *B* (2 min), injection volume: 1 mL, sample size: 2 × 3 mg in 1 mL H_2O/MeCN (1:1). *HPLC-Method IV: Agilent*. Column: *Machery Nagel Nucleodur Sphinx*, 46 × 150 mm, 5 μm, 20 °C, λ = 254 nm, flow 1.4 mL/min, mobile phases for gradient elution phase *A* = 0.05% aq. TFA and phase *B* = MeCN, gradient: 55% *B* (5 min), 55 – 95% *B* (4.5 min), 95%. *HPLC-Method V: Agilent*. Column: *Machery Nagel Nucleodur Sphinx*, 8 × 150 mm, 5 μm, 20 °C, λ = 254 nm, 280 nm; flow 4.0 mL/min, mobile phases for gradient elution phase *A* = 0.05% aq. TFA and phase *B* = MeCN, gradient: 30% *B* (0 min), 36.5% *B* (6.5 min), 95% *B* (7 – 9.5 min), 30% *B* (10 min). *HPLC-Method VI: Agilent 1200*. Column *Waters Sunfire RP C18*, 4.6 × 150 mm, 5 μm, 40 °C, λ = 258 nm, flow: 1.0 mL/min, mobile phases for gradient elution phase *A* = H_2O/MeCN/TFA 95:5:0.1 (v/v) and phase *B* = H_2O/MeCN/TFA 5:95:0.1, gradient: 10% *B* (2 min), 40% *B* (15 min), 95% *B* (16 min), 95% *B* (20 min), 95% *B*(20.1 min), 10% *B* (25 min), sample: 0.2 – 0.4 mg/mL in MeCN/H_2O 1:1. *HPLC-Method VII*: *Agilent 1200*. Column *Diacel OD-H*, 2.1 × 150 mm, 5 μm, 30 °C, λ = 240 nm, flow: 1.0 mL/min, mobile phase *A* = HEX/IPA/EtOH 95:2.5:2.5 (v/v/v) and mobile phase *B* = IPA/EtOH 1:1, isocratic for 45 min, *A*/*B* 95:5. For HPLC-methods VI and VII a *Berthold LB509* radio detector with a 100 μL Z-cell was used in all cases. Scintillation cocktails either were *Perkin Elmer*'s *Flow-Scint A* (3.0 mL/min) or *Zinsser*'s *Quickzint Flow 302* (2.8 mL/min). *UPLC/MS Method.* Electrospray ionization positive mode. Column: *Acquity HSS T3* 1.8 μm, 2.1 × 50 mm at 60 °C; eluent *A*: water + 0.05% formic acid + 3.75 mM NH_4OAc; eluent *B*: MeCN + 0.04% formic acid; gradient from 5 to 98% *B* in 1.4 min, flow 1.0 mL/min. In case of method VII, the limit of detection (LOD) was set to a signal to noise ratio (SN) of 3. All peaks ≥ LOD were detected.

NMR. Chemical shifts (δ) are given in ppm referenced to the residual solvent peak. Multiplicities are abbreviated as follow: *s* = *singulet*, br. = broad, *d* = *doublet*, *dd* = *doublet* of a *doublet*, *dq* = *doublet* of a *quadruplet*,

Table 5. ^{1}H-NMR data for compound CDZ173 (**1a**)

Conformer I, $\delta(^1H)$ [ppm]		Mixed form of conformer[a], $\delta(^1H)$ [ppm]	
H–C(2‴)	8.28 (*d*, ^4J = 2.81)	H–C(2‴)	8.28 (*d*, ^4J = 2.81)
H–C(2″)	8.35 (*s*)	H–C(2″)	8.34 (*s*)
H–C(4‴)	7.87 (*d*, ^4J = 3.00)	H–C(4‴)	7.87 (*d*, ^4J = 3.00)
NH	6.76 (*d*, ^3J = 6.43)	NH	6.73 (*d*, ^3J = 6.10)
H–C(3′)	4.70 (*pseudo-sext.*,^2J = 6.57, ^3J = 6.60)	H–C(3′)	4.58 (*dt*, ^2J = 6.35, ^3J = 6.38)
CH_2(5″)	3.97 (*s*)	CH_2(5″)	3.97 (*s*)
MeO–C(6‴)	3.92 (*s*)	MeO–C(6‴)	3.92 (*s*)
H′–C(2′)	3.84 (*dd*, ^2J = 10.42, ^3J = 6.90)	H′–C(2′)	3.71 (*dd*, ^2J = 11.99, ^3J = 6.93)
H′–C(5′)	3.55 (*dd*, ^2J = 7.67, ^3J = 5.54)	H′–C(5′)	3.60 (*ddd*, ^2J = 10.25, ^3J = 7.64, ^3J = 5.89)
CH_2(7″)	3.52 (*dd*, ^2J = 6.78, ^3J = 6.78)	CH_2(7″)	3.52 (*dd*, ^2J = 6.78, ^3J = 6.78)
H″–C(5′)	3.37 (*m*)	H″–C(5′)	3.50 (*d*, ^2J = 7.96)
H″–C(2′)	3.33 (*dd*, ^2J = 10.75, ^3J = 4.81)	H″–C(2′)	3.29 (*dd*, ^2J = 12.06, ^3J = 5.62)
CH_2(8″)	2.80 (*m*)	CH_2(8″)	2.80 (*m*)
CH_2(2)	2.20 (*m*)	CH_2(2)	2.26 (*q*, ^3J = 7.40)
H′–C(4′)	2.15 (*dq*, ^2J = 12.64, ^3J = 6.14)	H′–C(4′)	2.22 (dt, ^2J = 7.38, ^3J = 3.90)
H″–C(4)	1.92 (*dq*, ^2J = 12.74, ^3J = 7.45)	H″–C(4)	2.01 (*dq*, ^2J = 13.88, ^3J = 6.99)
Me(3)	0.98 (*m*)[b]	Me(3)	0.98 (*m*)[b]

[a] Refers to a conformation where the propionly side chain is periplanar to the pyrroldine ring (see cross peaks, *Figure 5* main part). [b] *q* overlaid with *dd*.

dquint. = *doublet* of a *quintuplet*, exch. = exchangeable, *t* = *triplet*, *sext.* = *sextuplet*. 400 MHz ^{1}H-NMR spectra were recorded on *VNMRS-400* at 296 K. 600 MHz Spectra on *Bruker DRX600* with 1.7 mm-cryoprobe *TCI-C/N* probe head. ^{3}H-NMR spectra of compound **1b** were acquired on *Bruker DPX400* with *SXI-3H* probe head using a registered sample of the phosphate salt of **1a** ($[C_{21}H_{26}F_3N_6O_2]^+[H_2PO_4]^-$, 548.85 g/mol) as external reference for NMR-difference spectroscopy. ^{13}C-NMR Shifts were extracted from the HMBC and HSQC data set as much as possible. Processing and assignment software in all cases: XWin NMR and MNova v11.0.6 (MestreReNova). Qualitative conformational analysis of **1a** (CDZ173) was done based on the ROESY datasets. ^{1}H- and ^{13}C-coupling constants (^nJ) are given in Hz indicating the bond order *n*. ROESY spectra of **22** were smoothed with the *Savitzky–Golay* method and denoised with the *Gaussian* method. Numbering of protons and carbons in the experimental part is in line with the IUPAC name of the compounds.

NMR of CDZ173 (**1a**). ^{1}H-NMR (^{1}H, COSY, TOCSY, HSQC, HMBC, ROESY, (D_6)DMSO, 22 °C): See *Table 5*. See also *Scheme 4* and *Figure 5* in main text to align with given MNova atom numbering (*Figure 6*). ^{13}C-NMR (^{13}C, HSQC, HMBC, (D_6)DMSO, 25 °C): See *Table 6*.

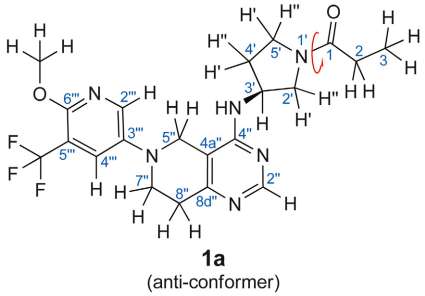

Figure 6. Atom numbering of compound **1a** (anti-conformer is shown).

Synthetic Procedures and Analytical Data

6-Benzyl-5,6,7,8-tetrahydropyrido[4,3-*d*]pyrimidin-4-ol (**2**).[11][51] To a solution of methyl 1-benzyl-4-oxopiperidine-3-carboxylate (6.4 g, 25.9 mmol) in MeOH (300 mL) was added acetic acid methanimidamide (4.04 g, 38.8 mmol) in MeOH (10 mL) and 0.5 M MeONa in MeOH (207 mL, 104 mmol). Subsequently, the solution was stirred for 3 h at 90 °C (oil bath) while being monitored by UPLC/MS. Then CH_2Cl_2 (*ca.* 300 mL) and AcOH (5.9 mL, 6.22 g, 104 mmol) were added and the mixture was stirred over night at r.t. The reaction was quenched with water and extracted with CH_2Cl_2 (1 × 500 mL) and CH_2Cl_2/IPA (3:1, 2 × 500 mL). The organic layers were combined, dried over Na_2SO_4, and concentrated under vacuum. The residue was purified by automated flash chromatography eluting with CH_2Cl_2/1 – 10% MeOH gradient. This resulted in 5.2 g (83%) of **2** as acetic acid salt (> 95% UV on UPLC/MS) UPLC/MS (ESI+): 242.1 (100, $[M + H]^+$; calc. 242.13), 243.3 (15, $[M + H]^+$; calc. 243.13).

Table 6. ^{13}C-NMR (^{13}C, HSQC, HMBC, (D$_6$)DMSO, 25 °C)

Conformer I, δ(^{13}C) [ppm]		Mixed form of conformer[a], δ(^{13}C) [ppm]	
C(1)	171.21	C(1)	171.11
C(3‴)	141.20	C(3‴)	141.20
C(4″)	158.04 or 158.00[b]	C(4″)	158.00 or 158.04
C(8d″)	158.51 or 158.41[a]	C(8d″)	158.41 or 158.51
C(2″)	155.43	C(2″)	155.43
C(6‴)	153.55	C(6‴)	153.55
C(2‴)	137.90	C(2″)	137.90
C(4‴)	125.55	C(4‴)	125.55
CF_3	123.20 (*q*, ^1J(C,F) = 271.97)	CF_3	123.20 (*q*, ^1J(C,F) = 271.97)
C(5‴)	111.06 (*q*, ^2J(C,F) = 32.23)	C(5‴)	111.06 (*q*, ^2J(C,F) = 32.23)
C(4a″)	109.64 or 109.62[a]	C(4a″)	109.62 or 109.64
MeO–C(6‴)	53.65	MeO–C(6‴)	53.65
C(2′)	50.91	C(2′)	50.26
C(3′)	50.72	C(3′)	49.33
C(5″)	45.81 or 45.79[c]	C(5″)	45.81 or 45.79
C(7″)	45.79 or 45.81[b]	C(7″)	45.79 or 45.81
C(5′)	43.65	C(5′)	44.24
C(8″)	31.18	C(8″)	31.18
C(4′)	29.63	C(4′)	31.34
C(2)	26.89	C(2)	26.53
C(3)	8.90	C(2)	8.90

[a] Refers to a conformation where the propionly side chain is periplanar to the pyrroldine ring (see cross peaks, *Figure 5* main part). [b] Undistinguishable carbons of conformers. [c] Undistinguisbale carbons.

6-benzyl-4-chloro-5,6,7,8-tetrahydropyrido[4,3-*d*]-pyrimidine (**3**). In an inert atmosphere, compound **2** (acetic acid salt, 4 g, 1.63 mmol) was dissolved in toluene (50 mL) and Et_3N (4.62 mL, 33.2 mmol) was added. $POCl_3$ (2.32 mL, 24.9 mmol) was added dropwise. The mixture was stirred at 100 °C (oil bath), while the reaction was monitored by UPLC/MS. After 2 h, the mixture was cooled to r.t., the reaction was quenched with $NaHCO_3$ (20 g), the resulting mixture was stirred for 1 h, filtered, and evaporated. The residue was dissolved in water (200 mL), pH was adjusted with sat. $NaHCO_3$ to pH 8 and extracted with CH_2Cl_2 (3 × 200 mL). The combined organic layers where dried over Na_2SO_4, filtered, and evaporated to dryness to yield **3** (2.5 g, 58%) ^{1}H-NMR ((D$_6$)DMSO): 8.76 (*s*, 1 H); 7.34 – 7.25 (*m*, 5 H); 3.73 (*s*, 2 H); 3.54 (*s*, 2 H); 2.89 (*m*, 2 H); 2.77 (*m*, 2 H). UPLC/MS (method 1): (100, $[M + H]^+$; calc. 260.10), 262.1 (31, $[M + H]^+$; calc. 262.10), 263.2 (5, $[M + H]^+$; calc. 263.10).

(*S*)-*tert*-Butyl (1-Propanoylpyrrolidin-3-yl)carbamate (**5**). (*S*)-*tert*-butyl pyrrolidin-3-ylcarbamate[52] (**4**; 2 g, 10.7 mmol) was dissolved in THF (20 mL). Et_3N (1.96 mL, 14.0 mmol) and propanoyl chloride (1.1 g, 11.8 mmol) were added. The resulting solution was stirred for 2 h at r.t. when UPLC/MS indicated completion of the reaction, and the mixture was quenched with sat. aq. $NaHCO_3$ (20 mL). The mixture was extracted with AcOEt (3 × 50 mL), the combined organic phases were dried over Na_2SO_4, filtered, and concentrated under vacuum to yield **5** (2.4 g, > 95% UV). UPLC/MS (ESI+): 265.2 (15, $[M + Na]^+$; calc. 265.15), 187.1 (100, $[(M - {}^t\text{Bu}) + H]^+$; calc. 187.11).

1-[(3*S*)-3-Aminopyrrolidin-1-yl]propan-1-one (**6**). Compound **5** (2.4 g, 9.90 mmol) was dissolved in CH_2Cl_2 (15 mL). Then, 4 N HCl in dioxane (15 mL, 60.0 mmol) were added, and the solution was stirred for 2 h when UPLC/MS indicated completion. The mixture was concentrated, dissolved in MeCN (20 mL), and solid K_2CO_3 (10 g) was added. The mixture was stirred overnight, then filtered, and the filtrate was evaporated to yield **6** (1.41 g, quant.) UPLC/MS (ESI+): 165.2 ($[M + Na]^+$; calc. 165.10).

1-{(3*S*)-3-[(6-Benzyl-5,6,7,8-tetrahydropyrido[4,3-*d*]-pyrimidin-4-yl)amino]pyrrolidin-1-yl}propan-1-one (**7**). In a microwave vial, compound **3** (480 mg, 185 μmol), (*S*)-**6** (263 mg, 185 μmol), and cat. AcOH (31.7 μL, 0.55 μmol) were dissolved in EtOH (10 mL). The mixture was ramped for 20 min at 200 W to 110 °C, then slightly concentrated in the vacuum, and heating was continued in an oil bath at 140 °C for 18 h. When UPLC/MS control indicated end of reaction, the solvent was evaporated, the resulting mixture dissolved in CH_2Cl_2 (10 mL) and injected into the automated flash chromatography system (CH_2Cl_2/0 – 10% MeOH gradient). 260 mg of **7** were obtained (38%, *ca.* 80% UV on

UPLC/MS). In a scale up batch, **3** (14.4 g, 55.44 mmol) and (*S*)-**6** (10.2 g, 71.7 mmol, 1.30 equiv.) were placed into a 250-mL round-bottom flask and dissolved in EtOH (200 mL). Then, AcOH (0.953 μL, 16.6 mmol, 0.30 equiv.) was added, and the solution was stirred overnight at 140 °C (oil bath). The solution was cooled to 25 °C, diluted with CH_2Cl_2 (100 mL) and concentrated under vacuum. The residue was applied on a silica gel column and eluted with a CH_2Cl_2/MeOH gradient (1 – 15% MeOH). 17 g of **7** (84%) were obtained. UPLC/MS (ESI+): 366.2 (100, $[M + H]^+$; calc. 366.23), 367.2 (10, $[M + H]^+$; calc. 267.23).

1-[(3*S*)-3-(5,6,7,8-Tetrahydropyrido[4,3-*d*]pyrimidin-4-ylamino)pyrrolidin-1-yl]propan-1-one (**8**). Compound **7** (260 mg, 0.71 mmol) was dissolved in EtOH (10 mL), and $Pd(OH_2)$ on carbon (110 mg) was added. The system was stirred in a mixed atmosphere of hydrogen and air for 18 h at 60 °C. The catalyst was removed by filtration, the filtrate was evaporated, and the residue was purified by automated flash chromatography (CH_2Cl_2/0 – 10% MeOH gradient). 78 mg of compound **8** (40%, *ca*. 90% UV on UPLC/MS) were obtained. In a scale up batch, **7** (17 g, 46.5 mmol, 1.00 equiv.) was placed into a 250-mL round-bottom flask and dissolved in EtOH (150 mL). $Pd(OH)_2$ on carbon (6 g) was added, the flask was closed with a rubber stopper, the suspension was frozen in liquid N_2, and the flask was evacuated in the high vacuum. Hydrogen gas was expanded into the flask using the balloon technique for gas transfer, the suspension was thawed up and stirred overnight at 60 °C (oil bath). Subsequently, the solids were filtered and the resulting mixture was concentrated under vacuum giving 11 g of compound **7**. UPLC/MS (ESI+, *m/z*): calculated for $C_{14}H_{21}N_5O$ 276.2 (100, $[M + H]^+$; calc. 276.18), 277.1 (13, $[M + H]^+$; calc. 277.19).

***tert*-Butyl 4-{[(3*S*)-1-Propanoylpyrrolidin-3-yl]amino}-7,8-dihydropyrido[4,3-*d*]pyrimidine-6(5*H*)-carboxylate** ((*S*)-**9**, ee = 100%). Compound **8** (11 g, 40 mmol) was placed in a 500 mL-round-bottom flask and dissolved in CH_2Cl_2 (100 mL). Et_3N (12 g, 118.6 mmol) was added. Then di-*tert*-butyl dicarbonate (12.4 g, 56.8 mmol) was added at 0 °C and the solution was stirred for 3 h at r.t. The reaction was then quenched with water (100 mL) and the suspension was extracted with CH_2Cl_2 (3 × 200 mL). The organic layers were combined, dried over Na_2SO_4, and concentrated under vacuum. The residue was applied onto a silica gel column and eluted with CH_2Cl_2/MeOH gradient (1 → 15%) to get 10 g of **9** (ee = 95.1% with HPLC-method I). This product (10 g) was purified by chiral semi-prep. HPLC using HPLC-method II to get 7.9 g of (*S*)-**9** (ee < 99% with HPLC-method I; (*S*)/(*R*) = 100:0 ((*R*)-enantiomer undetectable with HPLC method 1)). For assignment of the absolute configuration of the (*S*)-isomer, (*R*)-**9** was synthesized independently from (*R*)-**4** as described for (*S*)-**6** from (S)-**4**. With HPLC-method I, a 1:1 mixture of (S)-**9** and (*R*)-**9** gave baseline separation of the isomers with t_R((*R*)-**9**) = 9.263 and t_R((*S*)-**9**) = 13.908 (for the mixture (*R*)/(*S*) = 49.57:50.43). MS (ESI^+): 376 ($[M + H]^+$; calc. 376.23).

1-[(3*S*)-3-(5,6,7,8-Tetrahydropyrido[4,3-*d*]pyrimidin-4-ylamino)pyrrolidin-1-yl]propan-1-one ((*S*)-**8**, ee > 99%). Compound (*S*)-**9** (6.0 g, ee = 100%, 15.98 mmol) was placed into a 500 mL 3-necked round-bottom flask and dissolved in Et_2O (500 mL). Into this solution, dry HCl gas was introduced, and the mixture was stirred for 2 h at r.t. The solids were collected by filtration, and the filter cake was washed with Et_2O (3 × 50 mL). The crude product was recrystallized from 10% MeOH in Et_2O (100 mL). The collected material was dissolved in water (50 mL), the solution was neutralized with 1 M NaOH (2 equiv.) and lyophilized. Subsequently, the product was dissolved in THF/1% MeOH (500 mL), and the precipitate of NaCl was removed by filtration. The filtrate was concentrated under vacuum and the product dried in the high vacuum to yield 2.97 g (64%) of (*S*)-**8**. Since non-racemizing conditions were used for deprotection, the optical purity of basic (*S*)-**8** (ee > 99%) was deduced from the optical purity of the less basic (*S*)-**9** (ee > 99%). ^{1}H-NMR, COSY, HSQC ((D_6)DMSO, *T* = 296 K): For conformer A, see *Table 7*, for conformer B, see *Table 8*. Atom numbering is depicted in *Figure 7*. ^{1}H-NMR ((D_6)DMSO, *T* = 373 K): For a single conformer, see *Table 9*. HighRes-MS (ESI^+): 276.18175 (100, $[M + H]^+$; calc. 276.1824), 277.18487 (16, $[M + H]^+$; calc. 277.1858).

5-Bromo-4-iodo-2-methoxy-3-(trifluoromethyl)pyridine (**16**). Under N_2, LDA (4.75 mL, 9.5 mmol, *c* = 2.0 M in THF/HEP/EtPh) was added to THF (4.75 mL) kept at –85 to –95 °C. Then, a solution of 5-bromo-2-methoxy-3-(trifluoromethyl)pyridine (9.5 mmol, 2.43 g) in THF (5.5 mL) was added dropwise. Finally, a catalytic amount of anhydrous LiBr (0.95 mmol, 82.5 mg) was added, and the mixture was kept at –85 to –95 °C for 180 min. Then, a solution of I_2 (1.35 mmol, 3.43 g) pre-cooled to –85 to –95 °C was added in small portions to the lithiated species using a Ar-filled graduated pipette. The mixture was kept for further 60 min at –85 to –95 °C and then warmed up to r.t. over night. After this time, the reaction was quenched with 1% aq. $Na_2S_2O_3$ (20 mL) and extracted with CH_2Cl_2 (3 × 50 mL). The combined organic phases were washed with 5% aq. $Na_2S_2O_3$ until they were colorless, then dried over $MgSO_4$ and

Table 7. ^{1}H- and ^{13}C-NMR data for conformer A of (*S*)-**8**, at 296 K

$\delta(^1H)$ [ppm]		$\delta(^{13}C)$ [ppm]	
H–C(2″)	8.28 (*s*)	C(2″)	156.2
NH	6.57 (*d*, ^3J = 12.0)	–	–
H_α–C(3′)	4.65 (*pseudo-sext.*, ^3J = 6.3)	C(3′)	51.2
H′–C(2′)	3.77 (*dd*, ^2J = 9.9, ^3J = 7.0)	C(2′)	51.4
CH_2(5″)	3.60 (br. *s*)	C(5″)	42.1
H′–C(5′)	3.45 (*m*)	C(5′)	44.0
H″–C(5′)	3.35 (*m*)	–	–
H″–C(2′)	3.32 (*m*)	C(2′)	51.4
CH_2(7″)	3.01 (*m*)	C(7″)	42.5
CH_2(8″)	2.58 (*m*)	C(8″)	31.2
CH_2(2)	2.24 (*q*, ^3J = 7.5)	C(2)	27.0
H′–C(4′)	2.07 (*m*)	C(4′)	29.9
H″–C(4)	1.90 (*m*)	–	–
Me(3)	0.99 (*t*, ^3J = 6.7)	C(3)	9.3

Table 8. ^{1}H- and ^{13}C-NMR data for conformer B of (*S*)-**8**, at 296 K

$\delta(^1H)$ [ppm]		$\delta(^{13}C)$ [ppm]	
H–C(2″)	8.28 (*s*)	C(2″)	156.2
NH	6.54 (*d*, ^3J = 11.5)	–	–
H_α–C(3′)	4.50 (*pseudo-sext.*, ^3J = 6.0)	C(3′)	49.6
H′–C(2′)	3.64 (*m*)	C(2′)	50.7
CH_2(5″)	3.60 (br. *s*)	C(5″)	42.1
H′–C(5′)	3.55 (*m*)	C(5′)	44.5
H″–C(5′)	3.49 (*m*)	–	–
H″–C(2′)	3.27 (*m*)	C(2′)	50.7
CH_2(7″)	3.01 (*m*)	C(7″)	42.5
CH_2(8″)	2.58 (*m*)	C(8″)	31.2
CH_2(2)	2.20 (*m*)	C(2)	27.0
H′–C(4′)	2.16 (*m*)	C(4′)	31.6
H″–C(4)	2.00 (*m*)	–	–
Me(3)	0.97 (*t*, ^3J = 6.8)	C(3)	9.3

evaporated. GC/MS of the crude material confirmed the presence of one single isomer in 60% yield (see *Supplementary Material 1.2.1*). For analytical purposes,

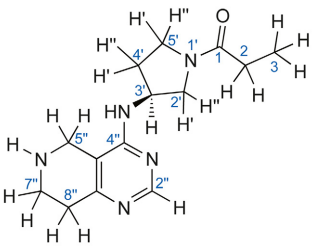

Figure 7. Atom numbering of compound (*S*)-**8**.

Table 9. ^{1}H-NMR data of one single conformer ((D_6)DMSO) at T = 373 K

$\delta(^1H)$ [ppm]	
H–C(2″)	8.25
NH	6.21 (*s*, large)
H_α–C(3′)	4.61 (*m*)
H′–C(2′)	3.8 – 3.1 (*m*)
CH_2(5″)	3.65 (*s*)
H′–C(5′)	3.8 – 3.1 (*m*)
H″–C(5′)	3.8 – 3.1 (*m*)
H″–C(2′)	3.8 – 3.1 (*m*)
CH_2(7″)	3.03 (*t*, ^2J = 6.0)
CH_2(8″)	2.60 (*t*, ^2J = 6.0)
CH_2(2)	2.22 (*m*)
H′–C(4′)	2.1 – 1.8 (*m*)
H′–C(4′)	2.1 – 1.8 (*m*)
Me(3)	1.01 (*t*, ^3J = 6.9)

an aliquot of this material was purified by chromatography. In a second experiment, a solution of 5-bromo-2-methoxy-3-(trifluoromethyl)pyridine (1.5 g, 5.85 mmol, 1 equiv.) in THF (11 mL) was cooled to −75 °C in a N_2-atmosphere. Then LDA (7.3 mL, 14.6 mmol, 2.5 equiv.) was added and the solution was stirred at −75 °C for 45 min. Subsequently, the mixture was poured into a solution of I_2 (5.95 g, 23.4 mmol, 4 equiv.) in THF (11 mL) cooled to 0 °C. Stirring was kept 5 min at 0 °C. Then 1% aq. $Na_2S_2O_3$ was added, and the mixture was extracted with Et_2O (2 × 100 mL). The combined organic layers were dried over Na_2SO_4 and evaporated to dryness. The residue was purified on silica gel (eluent: CYH) and the product was further purified by prep. HPLC on *Sunfire C18* (eluent: H_2O/0.1% HCO_2H in MeCN 6:4 → 4:6). The fractions containing compound **16** were extracted with Et_2O to give after drying (Na_2SO_4) and evaporation **16** (1 g, 45%, UV-UPLC > 99%). The configuration of **16** was confirmed by X-ray analysis[3] (see *Supplementary Material 1.2.2*). ^{1}H-NMR ((D_6)DMSO): 8.58 (*s*, 1 H); 3.94 (*s*, 3 H). ^{13}C-NMR ((D_6)DMSO): 159.4; 149.3; 123.1; 120.7; 118.9; 116.81 (*m*); 54.0. GC/MS (ESI^+): 380.8 (100, M^+; calc. 380.85), 381.8 (40, M^+; calc.

[3] Crystallographic data (excluding structure factors) for **16** – **18** have been deposited with the Cambridge Crystallographic Data Centre as supplementary publication number CCDC 1844455, CCDC 1844456 and CCDC 1844457. These data can be obtained free of charge *via* http://www.ccdc.cam.ac.uk/data_request/cif, by emailing data_request@ccdc.cam.ac.uk, or by contacting *The Cambridge Crystallographic Data Centre*, 12 Union Road, Cambridge CB2 1EZ, UK; fax: 441223 336033.

381.85), 382.8 (90, M^+; calc. 382.85), 383.8 (3, M^+; calc. 383.85).

4,5-Dibromo-2-methoxy-3-(trifluoromethyl)pyridine (**17**). Under N_2, a solution of 5-bromo-2-methoxy-3-(trifluoromethyl)pyridine (1.0 g, 3.9 mmol, 1 equiv.) in THF (10 mL) was cooled to −75 °C and LDA (2 M in Hex/ETPH, 3.9 mL, 7.8 mmol, 2 equiv.) was added, while controlling the temperature carefully during addition of the base. The solution was stirred at −75 °C for 1 h, then added to a solution of $C_2Br_2Cl_4$ (2.54 g, 7.8 mmol, 2 equiv.) in THF (10 mL) cooled to 0 °C. The solution was stirred for 3 min at 0 °C. Then, sat. aq. NH_4Cl (50 mL) was added. The mixture was extracted with AcOEt (3 × 100 mL), the combined organic layers were washed with brine, dried over Na_2SO_4, and evaporated to dryness. The residue was purified on silica gel (eluent: CYH) to give 0.8 g of **17** (60%, UV-HPLC 95%). The configuration of pure **17** was confirmed by X-ray analysis[4] (see *Supplementary Material 1.2.2*). ^{1}H-NMR ((D$_6$)DMSO): 8.70 (*s*, 1 H); 3.97 (*s*, 3 H). ^{13}C-NMR ((D$_6$)DMSO): 160.1; 151.7; 135.4; 117.2; 55.2. GC/MS (ESI$^+$): 334.8 (100, M^+; calc. 334.86), 332.8 (49, M^+; calc. 332.86), 336.8 (35, M^+; calc. 336.86).

5-Bromo-4-chloro-2-methoxy-3-(trifluoromethyl)pyridine (**18**). Under N_2, a solution of 5-bromo-2-methoxy-3-(trifluoromethyl)pyridine (1.0 g, 3.9 mmol, 1 equiv.) in THF (10 mL) was cooled to −75 °C and LDA (2 M in HEX/ETPH, 3.9 mL, 7.8 mmol, 2 equiv.) was added, while controlling the temperature carefully during addition of the base. The solution was stirred at −75 °C for 1 h, then added to a solution of C_2Cl_6 (1.84 g, 7.8 mmol, 2 equiv.) in THF (10 mL) cooled to 0 °C. The solution was stirred for 3 min at 0 °C. Then, sat. aq. NH_4Cl (50 mL) was added. The mixture was extracted with AcOEt (3 × 100 mL), the combined organic layers were washed with brine, dried over Na_2SO_4, and evaporated to dryness. The residue was purified on silica gel (eluent: CYH) to give 0.55 g of **18** (48%, UV-HPLC *ca.* 95%). The configuration of pure **18** was confirmed by X-ray analysis[4] (see *Supplementary Material 1.2.2*). ^{1}H-NMR ($CDCl_3$): 8.47 (*s*, 1 H); 4.03 (*s*, 3 H). GC/MS (ESI$^+$): 291.0 (100, M^+; calc. 290.91), 289.0 (28, M^+; calc. 288.91), 291.9 (5, M^+; calc. 291.91).

1-[(3*S*)-3-({6-[4-Chloro-6-methoxy-5-(trifluoromethyl)-pyridin-3-yl]-5,6,7,8-tetrahydropyrido[4,3-*d*]pyrimidin-4-yl}amino)pyrrolidin-1-yl]propan-1-one (**14**, *ee* > 99%). In an inert atmosphere, **18** (116 mg, 0.40 mmol), (*S*)-**8** (*ee* > 99%, 121 mg, 0.44 mmol), NaO^{t}Bu (57.6 mg, 0.6 mmol), Pd_2dba_3 (18.3 mg, 20 μmol), and ^{t}BuMePhos (7.48 mg, 20 μmol) are stirred in anhydr. ^{t}BuOH (4.0 mL) at r.t. Then, the mixture was stirred at 95 °C. In between 3 – 16 h, the reaction was followed by HPLC. When in process control indicated that the maximum amount of **14** was reached, the mixture was diluted with brine (10 mL) and extracted with AcOEt (2 × 20 mL). The combined organic layers were dried over Na_2SO_4, filtered, and evaporated to dryness. The residue was adsorbed on silica and added on top of a 10 g *SiOH chromabond* column. The product was eluted with a gradient of CH_2Cl_2 (100%) → CH_2Cl_2/MeOH/NH_4OH 98:2:1. The product fractions were further purified by HPLC using HPLC-method III. After lyophilization of the product fractions, 6 mg of **15** (UV-HPLC > 90%) were obtained. ^{1}H-NMR, COSY, ROESY, HSQC, HMBC ((D$_6$)DMSO, T = 296 K): see *Table 10*. For atom numbering, see *Figure 8*. ^{13}C-NMR: see *Table 11*. MS (ESI+): 485.0 (100, $[M + H]^+$; calc. 485.17), 487.0 (34, $[M + H]^+$; calc. 487.17), 486.0 (26, $[M + H]^+$; calc. 486.17), 488.0 (10, $[M + H]^+$; calc. 488.17).

1-[(3*S*)-3-({5,6,7,8-Tetrahydro-6-[6-methoxy-5-(trifluoromethyl)(4-^{3}H)pyridin-3-yl]pyrido[4,3-*d*]pyrimidin-4-yl}amino)pyrrolidin-1-yl]propan-1-one (**1b**). In a two-neck tritiation flask, Pd on C (10%, *BASF/Engelhard 4505*) and **22** (2.23 mg, 4.6 μmol) were suspended in DMF (800 μL), the flask was attached tightly to the tritium manifold, DIPEA (4.4 μL, 3.3 mg, 25.9 μmol) was added *via* the septum neck, and the flask was frozen in liquid nitrogen. Subsequently, the flask was degassed 3× in a freeze-thaw cycle. In the meanwhile, tritium gas was released at 775 K from the depleted uranium reservoir into the gas delivery arm (V = 4.5 mL) to give p = 1415 mbar (263 μmol) of tritium gas. The tritium gas was expanded at 291 K into the evacuated, frozen tritiation flask. After closing the reaction system at r.t., $p_{(291\ K)}$ = 353 mbar was observed in the volume above the frozen mixture corresponding to 202 μmol T_2. Once the mixture was thawed up and reached 291K, $p_{(t\ =\ 0)}$ = 603 mbar was observed in the volume above the mixture. After 12 min, the exothermic system equilibrated at T = 296 K and $p_{(t\ =\ 12\ min)}$ = 597 mbar. After 150 min at 296 K, gas up take stopped at $p_{(t\ =\ 150\ min)}$ = 591 mbar. The mixture was frozen until constant p = 334 mbar was reached in the volume above the frozen mixture corresponding to 10.9 μmol T_2 consumption ($\Delta p_{291\ K}$ = 19 mbar). The residual amount of tritium gas was pumped off the system into the recycling flow reservoir kept between 480 – 570 K, the reaction mixture was frozen in liquid N_2, the system was evacuated and the organic volatiles were lyophilized off. Volatile radioactivity in the vacuum dried crude product was expelled by suspending in MeOH (3 × 750 μL) and lyophilizing the carrier solvent into the waste ampule. The reaction flask was

Table 10. ^{1}H-NMR, COSY, ROESY, HSQC, HMBC ((D$_6$)DMSO, T = 296 K) of conformers A and B of compound **14**

Conformer A, $\delta(^1H)$ [ppm]		Conformer B, $\delta(^1H)$ [ppm]	
H–C(2‴)	8.48 (*s*)	H–C(2‴)	8.47 (*s*)
H–C(2″)	8.37 (*s*)	H–C(2″)	8.36 (*s*)
NH	6.66 (*d*, ^3J = 6.2)	NH	6.62 (*d*, ^3J = 5.8)
H$_\alpha$–C(3′)	4.68 (*pseudo-sext.*,^3J = 6.4)	H$_\alpha$–C(3′)	4.55 (*pseudo-sext.*,^3J = 6.0)
MeO–C(6‴)	3.96 (*s*)	MeO–C(6‴)	3.96 (*s*)
CH$_2$(5″)	3.91 (*s*)	CH$_2$(5″)	3.91 (*s*)
H′–C(2′)	3.80 (*dd*, ^2J = 10.5, ^3J = 6.8)	H′–C(2′)	3.65 (*dd*, ^2J = 12.0, ^3J = 6.8)
H′–C(5′)	3.42 (*m*)	H′–C(5′)	3.56 (*m*)
H″–C(5′)	3.41 (*m*)	H″–C(5′)	3.50 (*m*)
H″–C(2′)	3.31 (*m*)	H′–C(2′)	3.30 (*m*)
CH$_2$(7″)	3.32 (*m*)	CH$_2$(7″)	3.32 (*m*)
CH$_2$(8″)	2.82 (*t*, not resolved)	CH$_2$(8″)	2.82 (*t*, not resolved)
CH$_2$(2)	2.25 (*m*)	CH$_2$(2)	2.18 (*m*)
H′–C(4′)	2.11 (*m*)	H′–C(4′)	2.21 (*m*)
H″–C(4)	1.88 (*dq*, ^3J = 13.6, ^2J = 6.9)	H″–C(4)	1.98 (*dquint.*, ^2J = 13.1, ^3J = 6.6)
Me(3)	0.99 (*t*, ^3J = 7.4)	Me(3)	0.97 (*t*, ^3J = 7.9)

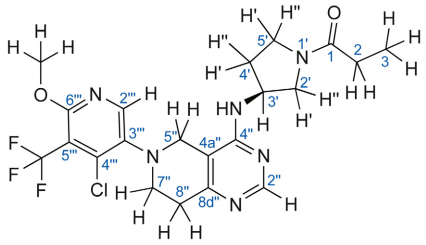

14

Figure 8. Atom numbering of compound **14**.

Table 11. ^{1}C-NMR ((D$_6$)DMSO, T = 296 K) of conformers A and B of compound **14**

Conformer A, $\delta(^{13}C)$ [ppm]		Conformer B, $\delta(^{13}C)$ [ppm]	
C(1)	171.51	C(1)	171.51
C(3‴)	140.97	C(3‴)	140.97
C(4″)	158.20	C(4″)	158.20
C(6‴)	157.60	C(6‴)	157.60
C(2″)	155.50	C(2″)	155.50
C(2‴)	144.70	C(2‴)	144.70
C(4‴)	141.00	C(4‴)	141.00
C(5‴)	n.d.	C(5‴)	n.d.
C(4a″)	110.47	C(4a″)	110.47
CF$_3$	n.d.	CF$_3$	n.d.
MeO–C(6‴)	54.98	MeO–C(6‴)	54.98
C(5″)	48.73	C(5″)	48.73
C(2′)	51.47	C(2′)	50.92
C(3′)	50.95	C(3′)	49.64
C(5′)	44.16	C(5′)	44.68
C(7″)	49.03	C(7″)	49.03
C(8″)	32.19	C(8″)	32.19
C(4′)	30.05	C(4′)	31.87
C(2)	27.05	C(2)	26.97

released from the manifold, the crude product was suspended in EtOH (*ca.* 5 mL in several portions), the suspension was filtered over a 0.2 μm *Whatman–Anotop* filter membrane into a graduated volumetric flask (200 mL) and toped up with MeOH to yield a stock solution of **1b** (1.295 MBq, 52% rad. chem. purity and product/educt ratio 1:2 (UV$_{\lambda\ =\ 254\ nm}$) on HPLC-method IV). From this stock solution, a first aliquot (200 μL) was purified by HPLC-method V to obtain 448 MBq tritiated **1b** in 10.84 mL eluent. This solution of **1b** was speed-vaced down to *ca.* 6 mL and neutralized with sat. aq. NaHCO$_3$. The compound was desalted on a 3 mL-*Strata X* column (100 mg sorbent) by washing with H$_2$O (2 × 2 mL) and eluting with EtOH to yield 306 μg of **1b** (426 MBq, 58% rad. chem. yield) in ethanol solution (*c* = 35.6 μg/mL, SA = 626.6 GBq/mmol, SA = 49.52 MBq/mL, HPLC-UV 100% (HPLC-method VI), HPLC-RA 96.8% (HPLC-method VI), chiral purity: 99.6%, ee = 99.2%, HPLC-method VII). The compound identity was confirmed by HPLC-co-injection with a registered reference sample of the phosphate salt of **1a** ($[C_{21}H_{26}F_3N_6O_2]^+[H_2PO_4]^-$, 548.45 g/mol) having chemo-physical characteristics as described in.[2] ^{3}H-NMR ((D$_6$)DMSO): 7.87 (*s*, 1 T). MS (**1a**; APCI$^+$): 450.4 (0.90), 451.2 (100, $[M + H]^+$, calc. 451.21), 452.2 (22.17, $[M + H]^+$, calc. 452.21), 453.2 (3.19, $[M + H]^+$, calc. 453.21). MS (**1b**; APCI$^+$): 450.4 (0.77), 451.3 (68.29), 452.4 (16.70), 453.2 (100, $[[^3H]M + H]^+$, calc. 453.22), 454.2 (22.81, $[[^3H]M + H]^+$, calc. 454.22), 455.2 (4.63, $[[^3H]M + H]^+$, calc. 455.22), 456.2 (0.59).

Dilution and Phosphate Salt Formation of **1b**. For biotransformation studies, aliquots of stock

solutions of pure **1b** were diluted with a stock solution of CDZ173-phosphate (2.474 μmol, 1.356 mg, *c*(EtOH) = 1.50 mg/mL) in a ratio 1:50. After co-evaporation and solubilization in MeCN/water 7:3, a 5 mM solution of [^{3}H]CDZ173 phosphate salt was obtained ($C_{21}H_{25}F_3N_6O_2$•H_3PO_4 (unlabeled), molecular weight (unlabeled) 548.5 g/mol, specific radioactivity 28.10 MBq/mg (free base) and 23.07 MBq/mg (as phosphate salt), 12.65 GBq/mmol (*i.e. ca.* 1% T-labelled); HPLC-RA: 99.3%, HPLC-UV: 99.1% both on HPLC-method VI). Remarks: A 4.3 μg sample of this material can be handelled in an uncontrolled lab. Due to the high dilution factor, the increase of the characteristic *m/z* 453.2 in **1b** was 18%. LC/MS (APCI$^+$) found for **1a** with $[(C_{21}H_{25}F_3N_6O_2)H]^+$ *m/z* 451.2 (100%), 452. (22.1%), **453.1 (3.10%)**, found for **1b** with $[(C_{21}H_{25}F_3N_6O_2)H]+$ *m/z* 451.2 (100%), 452.2 (22.9%), **453.2 (3.79%)**.

1-[(3*S*)-3-({5,6,7,8-Tetrahydro-6-[6-hydroxy-5-(trifluoromethyl)pyridin-3-yl]pyrido[4,3-*d*]pyrimidin-4-yl}amino)pyrrolidin-1-yl]propan-1-one (**19**). **1a** (111 μmol, 50 mg, free base) was dissolved in media *NL148S* (100 mL). Then, a culture of *streptomyces platensis* (1 mL) was added, and the mixture was shaken at 220 rpm/28 °C for 3 days. At this point, substrate conversion was 32% (LC/MS). Subsequently, NaCl (2 g) were added, and the mixture was extracted with Et_2O (3 × 100 mL). The organic phases were combined, dried over $MgSO_4$, filtered, evaporated under reduced pressure, and the crude material was dissolved in MeCN (10 mL). This solution was diluted with HPLC-eluent (H_2O/MeCN/formic acid 95:5:0.05) and applied onto a *Nucleodur RP18* (250 × 25 mm). Compound **19** eluted using a gradient H_2O/MeCN/formic acid 95:5:0.05 → H_2O/MeCN/formic acid 75:25:0.05. The fractions of **19** were combined, concentrated under reduced pressure, and lyophilized to yield pure **19** (12 mg, 27 μmol, 24% absolute; 76% rel. to conversion, 94% UPLC/DAD). ^{1}H-NMR ((D$_6$)DMSO, 303 K, 1:1 mixture of conformers A and B): 8.34 (*s*); 8.33 (*s*); 8.04 (br. *s*); 7.35 (*s*, exch.); 6.82 – 6.62 (*m*, exch.); 4.83 – 4.50 (*m*, conformers A and B); 3.73 (*s*); 3.63 – 3.34 (*m*); 2.81 – 2.75 (*m*); 2.34 – 2.11 (*m*); 0.99 (*q*, ^3J = 7.2). UPLC/MS (ESI+): 437.2 (100, $[M + H]^+$, calc. 437.19), 438.2 (24, $[M + H]^+$, calc. 438.19).

1-[(3*S*)-3-({5,6,7,8-Tetrahydro-6-[6-methoxy-5-(trifluoromethyl)pyridin-3-yl]-1-oxidopyrido[4,3-*d*]pyrimidin-4-yl}amino)pyrrolidin-1-yl]propan-1-one (**20**). Twelve shake flasks were filled with *NL148S* (200 mL each). To each flask, preculture of *Streptomyces griseus* (5 mL) was added and the flasks were shaken at 220 rom/28 °C for 2 days. After this time, a solution of CDZ173 (266 μmol, 120 g, free base) in MeCN/H_2O (22.2 mM, 12 mL, v/v 50:50) was prepared and aliquots of 1 mL (26.6 μmol/flask, 12.0 mg/flask) were added to each flask. Shaking was continued for additional 2 days at 220 rpm/28 °C when NaCl (42 g/flask) was added. Shaking was continued for additional 0.5 – 1 h. The culture solutions were combined and extracted with AcOEt (3 × 650 mL). The combined organic phases were dried over $MgSO_4$, filtered, and evaporated. The crude material was pre-purified on a custom made *RP18* stainless steel column (200 × 50 mm, stationary phase: *LiChroprep RP18* (*Merck KGaA 1.13900*)) using a flat gradient of *A* (H_2O/0.05% TFA) and *B* (MeCN/0.05% TFA); flow: 100 mL/min; 25 °C; λ = 264 nm; fraction size 60 mL. The product fractions were combined and concentrated under reduced pressure to *V* ≈ 250 mL. A second prep. HPLC purification was performed on *Sunfire RP18* (30 × 100 mm) using the gradient and detection conditions as described above (flow: 50 mL/min). The product fractions were combined, concentrated to *V* ≈ 150 mL and lyophilized to yield **20** (169 μmol, 79 mg, 37% absolute, > 96% HPLC/DAD). ^{1}H-NMR ((D$_6$)DMSO, 303 K, 1:1 mixture of conformers of A and B): 8.92 (*s*); 8.91 (*s*); 8.30 (*s*); 7.95 (*s*); 6.08 (*m*); 4.73 (*m*, conformer A); 4.63 (*m*, conformer B); 4.07 (*s*); 3.73 (*m*); 3.56 (*m*); 3.54 (*m*); 3.29 (*m*); 2.98 (*m*); 2.26 (*m*); 2.19 (*m*, conformer A); 2.08 (*m*, H′, conformer B); 1.99 (*m*, H″, conformer B); 1.00 (*m*). UPLC/MS (ESI+): 451.3 (18, $[M - O + H]^+$; calc. 451.21), 467.2 (100, $[M + H]^+$; calc. 467.20), 468.3 (40, $[M + H]^+$; calc. 468.21), 933.4 (5, $[2M + H]^+$; calc. 933.40).

1-[(3*S*)-3-({5,6-Dihydro-6-[6-methoxy-5-(trifluoromethyl)pyridin-3-yl]pyrido[4,3-*d*]pyrimidin-4-yl}amino)pyrrolidin-1-yl]propan-1-one (**21**) *and* **1-[(3*S*)-3-({5,6,7,8-Tetrahydro-5-(5*R*,*S*)-hydroxy-6-[6-methoxy-5-(trifluoromethyl)pyridin-3-yl]pyrido[4,3-*d*]pyrimidin-4-yl}amino)pyrrolidin-1-yl]propan-1-one** (**22**). A solution of **1a** (110 μmol, 50 mg) in MeCN (10 mL) was added to a solution of TEMPO (224 μmol, 35 mg) in *McIlvaine* buffer (500 mL, pH 4.5). Subsequently, laccase from *Trametes versicolor* (800 mg, > 10 U/mg, *SIGMA 51639*) was added and the suspension was incubated at 30 °C/160 rpm for 15 min. Afterwards NaCl (50 g) and NaOH (10 M, 5 mL) were added, the suspension was filtered and the filtrate was extracted with AcOEt (2 × 1 L). The combined organic phases were combined, dried over $MgSO_4$, filtered, and evaporated. The crude material was dissolved in MeCN/H_2O (60 mL, 5:1, v/v), diluted with eluent *A* and applied to *Sunfire RP18* (30 × 100 mm). Subsequent chromatographic separation of **21** and diastereomeric **22** using a gradient of *A* (H_2O/0.05% FA) and *B* (100% MeCN); flow: 100 mL/min; 25 °C; λ = 254 nm gave **21** (4.4 μmol, 4.5 mg, 4%) and

22 (33 μmol, 20 mg, 30%). The purity of dissolved **21** and **22** after chromatography was > 99% HPLC-UV. After fraction concentration and lyophilization, purity dropped to 50% in case of **21** and to 76% in case of **22**. *Analytical Data of* **21**: ^{1}H-NMR ((D$_6$)DMSO, 303 K, 1:1 mixture of conformers): 8.38 (*m*); 8.23 (*m*); 7.96 (*s*); 7.29 (*m*); 6.76 (*m*); 6.71 (*m*); 5.33 (*s*); 4.79 (br. *s*); 4.66 (*m*); 6.71 (*m*); 5.33 (*m*); 4.79 (br. *s*); 4.66 (*m*, conformer A); 4.53 (*m*, conformer B); 3.97 (*s*); 3.82 – 3.79 (*m*, conformer A); 3.70 – 3.68 (*m*, conformer B); 3.62 – 3.60 (*m*, conformer A); 3.55 – 3.50 (*m*, conformer B); 3.49 – 3.47 (*m*, conformer A); 3.34 – 3.25 (*m*); 2.27 – 2.19 (*m*); 2.17 – 2.13 (*m*); 2.12 – 2.04 (*m*, conformer A); 2.03 – 1.93 (*m*, conformer B); 0.97 (*m*). ^{13}C-NMR ((D$_6$)DMSO, 303 K, 1:1 mixture of conformers): 156.98; 138.57; 125.45; 138.57; 138.33; 137.43; 135.70; 125.45; 101.10; 54.26; 51.01; 50.71; 50.66; 49.61; 45.09; 44.54; 44.53; 43.97; 43.96; 31.62; 31.55; 29.94; 27.15; 26.90; 9.16. UPLC/MS (ESI+): 449.2 (100, $[M + H]^+$, calc. 449.19), 450.2 (23, $[M + H]^+$, calc. 450.19), 451.2 (2.5, $[M + H]^+$, calc. 451.19), 897.4 (5, $[2M + H]^+$, calc. 897.37). HighRes MS: 449.1913 (+ 0.9 ppm) fitting for $C_{21}H_{24}N_6O_2F_3^+$ with 99.59% confidence.

Analytical Data of **22**. ^{1}H-NMR ((D$_6$)DMSO, 303 K, 1:1 mixture of conformers and diastereoisomers): 8.40 (*s*); 8.30 (*s*); 7.89 (*s*); 6.63 (*m*, conformer A); 6.56 (*m*, conformer B); 6.10 (*m*); 5.90 (*m*); 3.94 (*s*); 3.84 – 3.69 (*m*); 3.54 – 3.45 (*m*); 3.31 (*m*); 2.91 (*m*, conformer A); 2.67 (*m*, conformer B); 2.26 – 2.10 (*m*); 2.03 (*m*, conformer A); 1.93 (*m*, conformer B); 0.99 (*m*). UPLC/MS (ESI+): 449.2 (100, $[(M - H_2O) + H]^+$), 450.2 (22, $[(M - H_2O) + H]^+$), 452.2 ($[M - (H_2O)]^+$), HighRes MS: 465.1866 (+ 0.9 ppm) fitting for $C_{21}H_{24}N_6O_2F_3$ with 99.73% confidence.

Incubation with Rat and Human Hepatocytes, Sample Preparation, and LC/MS^n Analytical Method

Material. [^{3}H]CDZ173 phosphate salt ($[C_{21}H_{25}F_3N_6O_2][H_3PO_4]$, 548.5 g/mol (unlabeled)) used for this hepatocyte incubation was the material described earlier in the experimental part. No further dilution was performed, however the purity of the stock solution was re-measured prior incubation by injection onto UPLC-RA system and was found to be 98.4%. A 5 μM stock solution of this material in H_2O/MeCN (3:7, v:v) was used. The cryopreserved rat hepatocytes used in this study had the following specifications: strain = *Sprague Dawley*, gender = male, supplier *Celsis*, product # *M00005*, lot # *LNZ*, number of pooled individuals = 17. The cryopreserved human hepatocytes used in this study had the following specifications: strain = mixed, gender = male and female, supplier = *Celsis*, product # *X008000*, lot # *PQP*, number of pooled individuals = 20. The cryopreserved hepatocytes were stored in liq. N_2. On the day of the incubations, the hepatocytes were thawed according to the instructions provided by the supplier.

Viability Measurements, Hepatocycte Incubations and Analytical Sample Preparation. In two parallel experiments, the cryopreserved hepatocytes (either rat or human origin as described above) were thawed, and the cells were suspended in serum-free *InVitroGRO HT* medium (*Celsis IVT*) using 25 mL tissue culture flasks (*Becton Dickinson Franklin Lakes*). At $t = 0$ min, the viability of the suspended hepatocytes was determined by a *Nucleocounter NC-200* (*Chemometec*) and was found to be 79.5% for rat hepatocytes and 80.0% for human hepatocytes. After cell counting, the cell density was adjusted to approx. 1×10^6 viable cells per mL by adding *InVitroGRO KHB* medium (*Celsis IVT*) to reach a total volume of each suspension of 4 mL. The incubations were started by adding 10 μL [^{3}H]CDZ173 phosphate salt as a solution in MeCN/DMSO/H_2O to each hepatocyte suspension. Incubates were shaken at 25 rpm and 37 °C under a humidified atmosphere of 95% air and 5% CO_2 in a *Heraeus* incubator/*Cytoperm*. The initial molar concentration of [^{3}H]CDZ173 in the incubates was 5 μM (corresponding to 413 kBq/mL) and the final concentration of DMSO in each incubate was below 0.5% (v/v). Aliquots of 250 μL were taken from either of the suspensions at $t = 0$ and $t = 240$ min (thus two samples of rat hepatocytes and two samples of human hepatocytes). At $t = 0$ and $t = 240$ min, the metabolic reaction in each sample was stopped by the addition of 500 μL volumes of ice-cold MeCN, each sample was vortexed and was kept at −20 °C overnight to assure the protein precipitation to be completed. Afterwards each sample was centrifuged for 20 min at 35 000 *g* (*Sigma 3K30* centrifuge, *Rotor# 12154*), and the pellet was separated from the supernatant. The supernatants of these four samples were decanted. In a negative control experiment the chemical stability of [^{3}H]CDZ173 under the incubation conditions was tested, *i.e.* [^{3}H]CDZ173 was incubated in 4 mL *InVitroGRO KHB* medium in the absence of hepatocytes and two aliquots were taken and analyzed as described above.

To determine the percentage radioactivity recoveries 20 μL weighted aliquots of each supernatant were transferred in a 6 mL LSC vial and a volume of 5 mL of scintillation cocktail (*Rialuma*, *Lumac*, The Netherlands) was added. The radioactivity was measured (up to

10 min measuring time) with a *Liquid Scintillation Analyzer* (*Tri-Carb*, *Packard Inst.*). The percentage radioactivity recoveries were 93.4 – 102.8% for metabolic patterns.

HPLC Methods for Metabolite Profiling and Identification. Up to 100 μL of each supernatant obtained after centrifugation were injected on a UPLC system equipped with a binary solvent manager (*C09UPB264M*), a photodiode array detector (*DAD D09UPD576M*) and a *Waters 2777* auto-sampler. The operating software monitoring the UPLC system was MassLynx Version 4.1 SCN627. Guard column: *Acquity UPLC HSS T3* 2.1 × 5 mm, 1.8 μm (*Waters*). Analytical column: *Acquity HSS T3* 1.8 μm, 2.1 × 150 mm (*Waters*). Column conditions: thermostated at 50 °C in a *Waters Acquity* column heater (*A09UPC403M*). Mobile phase *A* = 10 mM HCO_2NH_4, adjusted with HCO_2H to pH 3, mobile phase *B* = MeCN, Flow rate: 0.5 mL/min. Gradient (28 min total): 98% *A* + 2% *B* from 0.0 – 2.0 min; 98% *A* + 2% *B* to 88% *A* + 12% *B* from 2.0 – 2.1 min; 88% *A* + 12% *B* to 70% *A* + 30% *B* from 2.1 – 20.0 min, 2% *A* + 98% *B* from 24.0 – 25.5 min, 2% *A* + 98% *B* to 98% *A* + 2% *B* from 25.5 – 25.6 min, 98% *A* + 2% *B* from 25.6 – 28.0 min. After the DAD, the effluent was split 90:10 with 90% used for on-line radioactivity detection and 5% used for MS analysis. Before entering the radio-monitor *LB513* (*Berthold Technologies GmbH & Co. KG*, Bad Wildbad, Germany) equipped with a 100 μL flow cell, the effluent was mixed with 2.0 mL/min of *Rialuma* liquid scintillation cocktail (*Lumac*). The chromatograms are shown in *Figure 4*, main part of the manuscript. Baseline separating metabolites > 1% relative content were integrated.

LC MS, LC MS/MS, and Mass Analysis. The MS^n analysis of metabolites > 1% relative LC content was performed on MS instrumentation *Q-ToF Synapt I* mass spectrometer (*Waters*) operating under MassLynx™, version 4.1 SCN639 for instrument control, data acquisition and data processing. Ion source conditions: spray capillary 3.0 kV (ESI+), cone voltage 40V, nebulizer gas N_2 (7 bar), cone gas N_2 (25 L/h), desolvation gas N_2 (800 L/h), source block temperature 80 °C and desolvation temperature 180 °C. Collision activation: gas Ar (7.6×10^{-3} mbar), trap collision energy 6.0 eV (LC/MS) and 15 – 45 eV (LC/MS/MS), transfer collision energy 4 eV (LC/MS and LC/MS/MS). Mass analysis: Mass resolution *ca.* 9000 (full-width at half-maximum definition), V-mode (including accurate mass measurements), see *Supplementary Material* for the MS^1 and MS^2 of the metabolites and proposed fragmentation patterns.

Supplementary Material

Supporting information for this article is available on the WWW under https://doi.org/10.1002/hlca.201800044.

Acknowledgements

The team would like to thank, Dr. *Erich Grim* at *Pharmaron, Inc.* for contributing to the technical synthesis of amine (*S*)-**6**, Dr. *Bertrand Cottineau* at *Atlanchim Pharma*, Saint-Herblain (F) for the synthesis of **18** and **19** and Dr. *Christian Meisterhans*, *RC Tritec AG*, Teufen (CH) for providing several resynthesis of **1b** from **15**. *C. B.* would like to thank *Thomas Wolf*, *Christoph Bury*, *Emine Sager*, *Alexandre Luneau*, and *Kayhan Akyel* at *GDC Analytics* for the acquisition of analytical data. Additionally, *C. B.* would like to thank *Trixie Wagner* at *NIBR GCD Analytics* for the CCDC-submission of the crystal structures.

Author Contribution Statement

The manuscript and the *Supplementary Material* information were written by *C. B.* with contributions on biology by *Ch. Bu.*, metabolism and mass spectrometry by *D. P.* Radiosynthesis and the synthesis of **15** was accomplished by *T. L.* and *C. B.*; radio-analytics and release formulation were performed by *A. G.*, and *P. B.*; *C. H.* and *N. S.* synthesized (*S*)-**6**. X-Ray and GC-MS analytics concerning the configuration of **16**, **17**, and **18** were contributed by *I. D.* and *C. G.* Qualitative conformational analysis was done by *C. B. In vivo* rat studies were carried out by *S. D.* and *J.-C. Hengy*, microsome incubations, LC/MS and structure elucidation were performed by *J. B.*, *P. R.* and *W. G.* Hepatocyte incubations, LC/MS and structure elucidation were performed by *J. B.* and *K. L.* The metabolites **19** – **22** were synthesized by E. F.

Conflict of Interest

The authors contradict conflict of interests.

References

[1] M. Whitman, D. R. Kaplan, B. Schaffhausen, L. Cantley, T. M. Roberts, 'Association of Phosphatidylinositol Kinase Activity with Polyoma Middle-T Competent for Transformation', *Nature* **1985**, *315*, 239 – 242.

[2] K. Hoegenauer, N. Soldermann, F. Zécri, R. S. Strang, N. Graveleau, R. M. Wolf, N. G. Cooke, A. B. Smith, G. J. Hollingworth, J. Blanz, S. Gutmann, G. Rummel, A. Littlewood-Evans, C. Burkhart, 'Discovery of CDZ173 (Leniolisib), Representing a Structurally Novel Class of PI3K Delta-Selective Inhibitors', *ACS Med. Chem. Lett.* **2017**, *8*, 975 – 980.

[3] V. K. Rao, A. Christ, H. Su, A. Kashyap, S. Webster, A. Sediva, V. Dalm, P. M. Van Hagen, B. Sloth, M. J. Lenardo, M. Cabanski, C. Burkhart, G. Uzel, 'Successful Clinical Study of Leniolisib (CDZ173), a Small Molecule PI3K-Delta Inhibitor, in Patients with APDS/PASLI', *J. Clin. Immunol.* **2017**, *37*, 204 – 204.
[4] S.-M. Maira, F. Stauffer, J. Brueggen, P. Furet, C. Schnell, C. Fritsch, S. Brachmann, P. Chène, A. De Pover, K. Schoemaker, D. Fabbro, D. Gabriel, M. Simonen, L. Murphy, P. Finan, W. Sellers, C. García-Echeverría, 'Identification and Characterization of NVP-BEZ235, a New Orally Available Dual Phosphatidylinositol 3-Kinase/Mammalian Target of Rapamycin Inhibitor with Potent *In Vivo* Antitumor Activity', *Mol. Cancer Ther.* **2008**, *7*, 1851 – 1863.
[5] K. Hoegenauer, N. Soldermann, C. Hebach, G. J. Hollingworth, I. Lewis, von Matt A., A. B. Smith, R. M. Wolf, R. Wilcken, D. Haasen, C. Burkhart, F. Zécri, 'Discovery of Novel Pyrrolidineoxy-Substituted Heteroaromatics as Potent and Selective PI3K delta Inhibitors with Improved Physicochemical Properties', *Bioorg. Med. Chem. Lett.* **2016**, *26*, 5657 – 5662.
[6] K. Hoegenauer, N. Soldermann, F. Stauffer, P. Furet, N. Graveleau, A. B. Smith, C. Hebach, G. J. Hollingworth, I. Lewis, S. Gutmann, G. Rummel, M. Knapp, R. M. Wolf, J. Blanz, R. Feifel, C. Burkhart, F. Zécri, 'Discovery and Pharmacological Characterization of Novel Quinazoline-Based PI3K Delta-Selective Inhibitors', *ACS Med. Chem. Lett.* **2016**, *7*, 762 – 767.
[7] J. A. Krauser, 'A Perspective on Tritium Versus Carbon-14: Ensuring Optimal Label Selection in Pharmaceutical Research and Development', *J. Labelled Compd. Radiopharm.* **2013**, *56*, 441 – 446.
[8] F. P. Guengerich, 'Cytochrome P450 and Chemical Toxicology', *Chem. Res. Toxicol.* **2008**, *21*, 70 – 83.
[9] K. Levsen, H.-M. Schiebel, B. Behnke, R. Dötzer, W. Dreher, M. Elend, H. Thiele, 'Structure Elucidation of Phase II Metabolites by Tandem Mass Spectrometry: An Overview', *J. Chromatogr. A* **2005**, *1067*, 55 – 72.
[10] V. B. G. Reddy, G. A. Doss, B. V. Karanam, K. Samuel, T. J. Lanza Jr, L. S. Lin, N. X. Yu, A. S. Zhang, C. E. Raab, R. A. Stearns, S. Kumar, '*In Vitro* and *In Vivo* Metabolism of a Novel Cannabinoid-1 Receptor Inverse Agonist, Taranabant, in Rats and Monkeys', *Xenobiotica* **2010**, *40*, 650 – 662.
[11] E. Kretzschmar, P. Meisel, 'Synthese von 2,6-disubstituierten 4-hydroxy-5,6,7,8-tetrahydropyrido[4,3-d]pyrimidinen', *Pharmazie* **1988**, *43*, 475 – 476.
[12] F. Cottet, M. Marull, F. Mongin, D. Espinosa, M. Schlosser, 'Further Metalations and Functionalizations of Chloro-, Bromo- and Iodo(trifluoromethyl)pyridines', *Synthesis* **2004**, 1619 – 1624.
[13] F. Cottet, M. Schlosser, 'Three Chloro(trifluoromethyl)pyridines as Model Substrates for Regioexhaustive Functionalization', *Eur. J. Org. Chem.* **2004**, 3793 – 3798.
[14] M. Schlosser, 'CF_3-Bearing Aromatic and Heterocyclic Building Blocks', *Angew. Chem. Int. Ed.* **2006**, *45*, 5432 – 5446.
[15] Y. R. Luo, J. P. Cheng, in 'Bond Dissociation Energies in Polyatomic Cation', in 'CRC Handbook of Chemistry and Physics (Internet Version 2018)', 98th ed., Ed. J. R. Rumble, CRC Press/Taylor & Francis, Boca Raton, FL, 2018.
[16] J. P. Wolfe, S. L. Buchwald, 'Scope and Limitations of the Pd/BINAP-Catalyzed Amination of Aryl Bromides', *J. Org. Chem.* **2000**, *65*, 1144 – 1157.
[17] B. Basu, P. Das, A. K. Nanda, S. Das, S. Sarkar, 'Palladium-Catalyzed Selective Amination of Haloaromatics on KF-Alumina Surface', *Synlett* **2005**, 1275 – 1278.
[18] P. A. Fernandes Gomez Dos Santos, K. Högenauer, G. Hollingworth, N. Soldermann, F. Stowasser, N. Tufilli, F. Zecri, Patent WO 2013/001445, 03. Jan 2013.
[19] K. L. Davis-Bruno, A. Atrakchi, 'A Regulatory Perspective on Issues and Approaches in Characterizing Human Metabolites', *Chem. Res. Toxicol.* **2006**, *19*, 1561 – 1563.
[20] M. Kiffe, D. G. Schmid, G. J. M. Bruin, 'Radioactivity Detectors for High-Performance Liquid Chromatography in Drug Metabolism Studies', *J. Liq. Chromatogr. Relat. Technol.* **2008**, *31*, 1593 – 1619.
[21] G. Lappin, S. Temple, 'Radiotracers in Drug Development', Taylor & Francis, Boca Raton, FL, USA, 2006, pp. 18 – 39.
[22] R. Gretler, E. Askitoğlu, H. Kühne, M. Hesse, 'Die Massenspektrometrische *retro-Diels-Alder*-Reaktion: 1,2,3,4-Tetrahydroisochinolin und 1,2,3,4-Tetrahydronaphthalin (Tetralin). 31. Mitteilung über Massenspektrometrische Untersuchungen', *Helv. Chim. Acta* **1978**, *61*, 1730 – 1755.
[23] A. F. Ibañez, G. Y. M. Iglesias, 'Electron Impact Mass Spectrometry of Some 3-substituted 1,2,3,4-tetrahydroisoquinolines', *Org. Mass Spectrom.* **1991**, *26*, 132 – 134.
[24] A. M. M. Rawashdeh, C. Sotiriou-Leventis, X. R. Gao, N. Leventis, 'One-step Synthesis and Redox Properties of Dodecahydro-3a,9a-diazaperylene – the Most Easily Oxidized *p*-phenylenediamine', *Chem. Commun.* **2001**, 1742 – 1743.
[25] G. Dryhurst, P. J. Elving, 'Electrochemical Oxidation-reduction Paths for Pyrimidine Cytosine Purine and Adenine: Correlation and Application', *Talanta* **1969**, *16*, 855 – 874.
[26] J. F. O'Donnell, C. K. Mann, 'Controlled-potential Oxidation of Aliphatic Amides', *J. Electroanal. Chem.* **1967**, *13*, 157 – 162.
[27] F. Lozac'h, S. Fahrni, D. De Maria, C. Welte, J. Bourquin, H.-A. Synal, D. Pearson, M. Walles, G. Camenisch, 'Evaluation of cAMS for ^{14}C Microtracer ADME Studies: Opportunities to Change the Current Drug Development Paradigm', *Bioanalysis* **2018**, *10*, 321 – 339.
[28] S. E. Stein, in 'NIST Chemistry WebBook, NIST Standard Reference Database Number 69', Eds. P. J. Linstrom and W. G. Mallard, https://doi.org/10.18434/t4d303, (retrieved February 9, 2018), 2018.
[29] L. Carballeira, I. Pérez-Juste, '*Ab Initio* Study of the Pseudorotation and Conformational Stability of Pyrrolidine', *J. Chem. Soc., Perkin Trans. 2* **1998**, 1339 – 1345.
[30] C. Suarez, E. J. Nicholas, M. R. Bowman, 'Gas-Phase Dynamic NMR Study of the Internal Rotation in *N*-Trifluoroacetylpyrrolidine', *J. Phys. Chem. A* **2003**, *107*, 3024 – 3029.
[31] T. Husch, D. Seebach, A. K. Beck, M. Reiher, 'Rigorous Conformational Analysis of Pyrrolidine Enamines with Relevance to Organocatalysis', *Helv. Chim. Acta* **2017**, *100*, e1700182.
[32] E. J. Milner-White, L. H. Bell, P. H. Maccallum, 'Pyrrolidine Ring Puckering in *cis* and *trans*-proline Residues in Proteins and Polypeptides: Different Puckers are Favoured in Certain Situations', *J. Mol. Biol.* **1992**, *228*, 725 – 734.
[33] Y. K. Kang, J. S. Jhon, S. J. Han, 'Conformational Study of Ac-Xaa-Pro-NHMe Dipeptides: Proline Puckering and *trans/cis* Imide Bond', *J. Pept. Res.* **1999**, *53*, 30 – 40.

[34] C. Bauer, B. Jaun, 'Derivatives of Coenzyme F430 with a Covalently Attached α-axial Ligand. Part I – Evaluation of Suitable Spacer–Ligand Constructs by Molecular Modeling, Their Synthesis, and NMR Solution Structure', *Helv. Chim. Acta* **2003**, *86*, 4233 – 4253.
[35] C. Bauer, B. Jaun, 'Derivatives of Coenzyme F430 with a Covalently Attached α-Axial Ligand. Part II', *Helv. Chim. Acta* **2003**, *86*, 4254 – 4269.
[36] S. Gutmann, G. Rummel, B. Shrestha, (X-ray structure deposition authors), 'PDB ID 5O83. Ligand [9NQ]1101:A', RCSB Protein Data Base (retrieved from URL https://www.rcsb.org/3d-view/5O83/1 on 30-01-2018), **2017**.
[37] C. Wang, C. K. Moseley, S. M. Carlin, C. M. Wilson, R. Neelamegam, J. M. Hooker, 'Radiosynthesis and Evaluation of [^{11}C]EMPA as a Potential PET Tracer for Orexin 2 Receptors', *Bioorg. Med. Chem. Lett.* **2013**, *23*, 3389 – 3392.
[38] C. Bauer, Unpublished work: Labnote book entries E-43527-007 to E-43527-008 and E-43527-021 to E-43527-022, Novartis Pharma AG, 2009.
[39] R. P. Yu, D. Hesk, N. Rivera, I. Pelczer, P. J. Chirik, 'Iron-catalysed Tritiation of Pharmaceuticals', *Nature* **2016**, *529*, 195 – 199.
[40] A. A. Danopoulos, J. A. Wright, W. B. Motherwell, 'Molecular N_2 Complexes of Iron Stabilised by *N*-heterocyclic 'Pincer' Dicarbene Ligands', *Chem. Commun.* **2005**, 784 – 786.
[41] X. Huang, J. T. Groves, 'Beyond Ferryl-mediated Hydroxylation: 40 years of the Rebound Mechanism and C–H Activation', *J. Biol. Inorg. Chem.* **2017**, *22*, 185 – 207.
[42] P. M. Vignais, B. Billoud, J. Meyer, 'Classification and Phylogeny of Hydrogenases', *FEMS Microbiol. Rev.* **2001**, *25*, 455 – 501.
[43] T. Cresteil, B. Monsarrat, P. Alvinerie, J. M. Tréluyer, I. Vieira, M. Wright, 'Taxol Metabolism by Human Liver Microsomes: Identification of Cytochrome P450 Isozymes Involved in Its Biotransformation', *Cancer Res.* **1994**, *54*, 386 – 392.
[44] C. Markert, P. Rösel, A. Pfaltz, 'Combinatorial Ligand Development Based on Mass Spectrometric Screening and a Double Mass-Labeling Strategy', *J. Am. Chem. Soc.* **2008**, *130*, 3234 – 3235.
[45] J. Blanz, T. Délémonté, D. Pearson, A. Luneau, M. Ritzau, W. Gertsch, P. Ramstein, J. Dayer, S. Desrayaud, E. Braun, R. Aichholz, 'Micropreparative Isolation and NMR Structure Elucidation of Metabolites of the Drug Candidate 1-isopropyl-4-(4-isopropylphenyl)-6-(prop-2-yn-1-yloxy)quinazolin-2(1*H*)-one from Rat Bile and Urine', *J. Chromatogr. B* **2015**, *989*, 1 – 10.
[46] T. C. McIlvaine, 'A Buffer Solution for Colorimetric Comparison', *J. Biol. Chem.* **1921**, *49*, 183 – 186.
[47] M. Schlosser, in 'Organometallics in Synthesis: A Manual', John Wiley & Sons, Inc., 2013, pp. 1 – 166.
[48] E. Rapkin, G. Steele, R. Schavey, 'Modern Tritium Handling in the Synthesis Laboratory', *Am. Lab.* **1995**, *27*, 31 – 38.
[49] F. H. Spedding, A. S. Newton, J. C. Warf, O. Johnson, R. W. Nottorf, I. B. Johns, A. H. Daane, 'Uranium Hydride. 1. Preparation, Compostition and Physical Properties', *Nucleonics* **1949**, *4*, 4 – 15.
[50] V. T. Luu, J.-Y. Goujon, C. Meisterhans, M. Frommherz, C. Bauer, 'Synthesis of a High Specific Activity Methyl Sulfone Tritium Isotopologue of Fevipiprant (NVP-QAW039)', *J. Labelled Compd. Radiopharm.* **2015**, *58*, 188 – 195.
[51] K. Minamiguchi, S. Okajima, S. Aoki, M. Asai, T. Asai, H. Yamanaka, S. Dohi, 'Preparation of Novel Tetrahydropyridopyrimidine Compounds, and Antiandrogens and Antitumor Agents Containing Them', Taiho Pharmaceutical Co., Ltd., Japan, 2015, pp. JP5851663, paragraph 5850296.
[52] J. P. Sanchez, J. M. Domagala, C. L. Heifetz, S. R. Priebe, J. A. Sesnie, A. K. Trehan, 'Quinolone Antibacterial Agents. Synthesis and Structure–Activity Relationships of a Series of Amino Acid Prodrugs of Racemic and Chiral 7-(3-amino-1-pyrrolidinyl)quinolones. Highly Soluble Quinolone Prodrugs with *in Vivo* Pseudomonas Activity', *J. Med. Chem.* **1992**, *35*, 1764 – 1773.

Received March 23, 2018
Accepted April 25, 2018